New views on the emission and structure of the solar transition region

Hui Tian[a,b,*], Eckart Marsch[b], Chuanyi Tu[a], Werner Curdt[b], Jiansen He[b]

[a]*School of Earth and Space Sciences, Peking University, 100871, Beijing, China*
[b]*Max-Planck-Institut für Sonnensystemforschung, 37191 Katlenburg-Lindau, Germany*

Abstract

The Sun is the only star that we can spatially resolve and it can be regarded as a fundamental plasma laboratory of astrophysics. The solar transition region (TR), the layer between the solar chromosphere and corona, plays an important role in solar wind origin and coronal heating. Recent high-resolution observations made by *SOHO*, *TRACE*, and *Hinode* indicate that the TR is highly nonuniform and magnetically structured. Through a combination of spectroscopic observations and magnetic field extrapolations, the TR magnetic structures and plasma properties have been found to be different in coronal holes and in the quiet Sun. In active regions, the TR density and temperature structures also differ in sunspots and the surrounding plage regions. Although the TR is believed to be a dynamic layer, quasi-steady flows lasting from several hours to several days are often present in the quiet Sun, coronal holes, and active regions, indicating some kind of plasma circulation/convection in the TR and corona. The emission of hydrogen Lyman lines, which originates from the lower TR, has also been intensively investigated in the recent past. Observations show clearly that the flows and dynamics in the middle and upper TR can greatly modify the Lyman line profiles.

Keywords: Solar transition region, Coronal hole, Solar wind, UV radiation, Sunspots

1. Introduction

The Sun is the only star that we can spatially resolve. Observations suggest that many phenomena such as flares, particle acceleration, and collimated outflows not only occur in the solar atmosphere, but also occur in other astrophysical systems in similar forms (e.g., Zhang et al., 2000; Zhang, 2007). Thus, the Sun can be regarded as a fundamental plasma laboratory of astrophysics.

The solar transition region (TR), the temperature regime from ~10^4 K to 10^6 K, is traditionally believed to be a very thin layer between the solar chromosphere and corona. Figure 1 illustrates the structure of the solar interior and solar atmosphere, and shows the height variations of the temperature and density of the average solar atmosphere following the model of Vernazza et al. (1981). Abrupt changes of the temperature and density are clearly present through the TR. As an interface between the cool chromosphere and the hot corona, the TR plays an important role in coronal heating and solar wind origin (e.g., Chae et al., 1998b; Peter & Vocks, 2003; Tu et al., 2005a).

Most of the TR emission falls into the FUV/EUV range (~50 Å-2000 Å). And thus spectroscopic observations in this spectral range are the most important way to obtain information about the physics of the TR. Since the plasma is optically thin for most FUV/EUV emission lines, we can extract information about the physical conditions prevailing in their source regions from the line profiles (see reviews by Mariska, 1992; Xia, 2003; Wilhelm et al., 2007). Wavelengths and associated ions of several typical TR emission lines (the Mg x 625 Å line is formed in the lower corona) are marked in Figure 1 according to the formation temperatures of the ions (temperature of maximum fractional ionization). The TR can be divided into three parts according to the temperature: lower TR (10^4 K-3×10^4 K), middle TR (3×10^4 K-5×10^5 K), and upper TR (5×10^5 K-10^6 K). The lines of Lyα 1216 Å, He I 584 Å and Si II 1533 Å are all typical emission lines formed in the lower TR. The Ne VIII 770 Å line is a typical upper-TR line and has been widely used in observations in the last decade. In the middle TR, thousands of emission lines such as C II 1037 Å and C IV 1548 Å have been identified (Curdt et al., 2001), and many of them have been used in observations to probe the physical properties of the TR.

Early observations made by instruments such as the S082B EUV spectrograph onboard the Skylab space station (Bartoe et al., 1977), the UV spectrometer onboard the OSO 8 (Orbiting Solar Observatory) satellite (Bonnet, 1981), and the High-Resolution Telescope Spectrograph (HRTS) flown on some rockets and Spacelab 2 (Bartoe & Brueckner, 1975; Brueckner et al., 1986) have provided much valuable information about the solar TR. Early instruments and results of these early observations have been reviewed by Wilhelm et al. (2004) and Mariska (1992), respectively. However, our knowledge of the TR was limited due to the lack of long-duration high-resolution observations before middle 1990s.

With the launch of SOHO (Solar and Heliospheric Observatory), TRACE (Transition Region and Coronal Explorer), and Hinode, our understanding of the TR has been significantly improved since 1996. Huge amount of data acquired by these mis-

*Corresponding author
Email address: tianhui924@pku.edu.cn,tianhui924@gmail.com (Hui Tian)

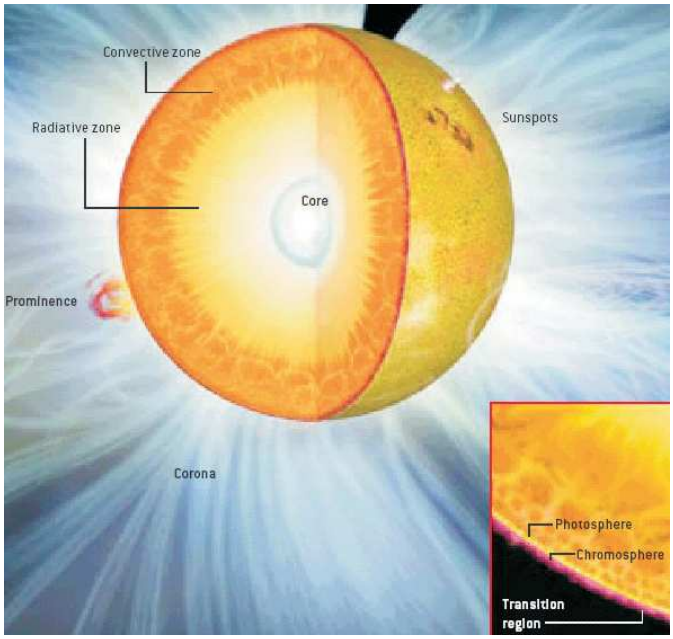

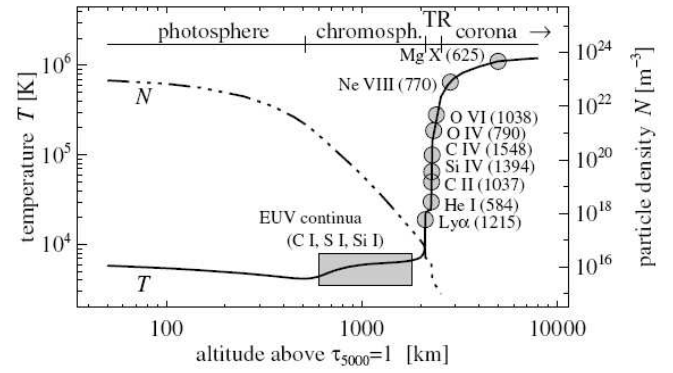

Figure 1: Upper: Structure of the solar interior and solar atmosphere. Adapted from the magazine of Scientific American (2003) and the thesis of McAteer (2004) (Credit: Don Dixon.). Lower: Height variations of the temperature and density of the average solar atmosphere. Adapted from Peter (2004).

sions reveal clearly that the TR is a highly dynamic and nonuniform layer. High spatial (∼1″), temporal (∼1 s), and spectral (1st order ∼44 mÅ/pixel, 2nd order ∼22 mÅ/pixel) observations of the SUMER (Solar Ultraviolet Measurements of Emitted Radiation) instrument (Wilhelm et al., 1995; Lemaire et al., 1997) onboard SOHO have greatly enhanced our knowledge of the TR. Thousands of emission lines with wavelengths from 660 Å to 1610 Å and formation temperatures from 10^4 K to 2×10^6 K have been identified and used in extensive studies of the upper solar atmosphere (Curdt et al., 2001, 2004). Moreover, the Doppler shifts of these FUV/EUV spectral lines could be measured with an accuracy of about 1-2 km/s (Brekke et al., 1997; Peter & Judge, 1999; Popescu et al., 2004), and thus the flow velocities in the TR could be determined with a high accuracy. Besides, the Coronal Diagnostic Spectrometer (CDS) onboard SOHO (Harrison et al., 1995) and the EUV Imaging Spectrometer (EIS) onboard Hinode (Culhane et al., 2007) have the capability of simultaneous multi-wavelength observations using a number of TR and coronal lines, which are very suitable for plasma diagnostics in the upper solar atmosphere.

Disk observations reveal that the bright network pattern is the dominant emission structure in intensity images of TR lines (e.g., Brueckner & Bartoe, 1974; Reeves, 1976). The TR network is cospatial with the underlying chromospheric network, and is believed to be the upward extension of the supergranular boundary to higher layers (e.g., Brueckner & Bartoe, 1974; Patsourakos et al., 1999). Reeves (1976) found that in the quiet Sun the contrast between the network and internetwork emission is largest for lines formed at $\sim 2 \times 10^5$ K and decreases at higher and lower temperatures. Patsourakos et al. (1999) investigated the height variation of the network size (width of the network lane) in the upper atmosphere of the quiet Sun, and found that the network size is almost constant in the middle TR and increases strongly at the upper TR. The TR is a low-β plasma region and the magnetic field largely controls the distribution of the plasma.

The first magnetic network model was proposed by Gabriel (1976). In this model, magnetic fields concentrated in the supergranular boundary expand with height and open into the corona. The TR radiation is balanced by the downward thermal conduction. However, the emission measure reproduced by this model is far less than the observed value at temperatures below 10^5 K (Athay, 1982). Ten years later, Dowdy et al. (1986) proposed a modified model in which only part of the network magnetic fields open into the corona as a funnel shape, while the rest of the network is occupied by a population of low-lying loops with lengths less than 10 Mm (1 Mm=10^6 m). In this model, the small loops are heated internally. Peter (2001) further pointed out that magnetic funnels originating from the network could be connected to the solar wind or be legs of large-scale coronal loops. It might also be possible that the fundamental structure of the TR has not yet been resolved due to limitations of current instruments (Feldman, 1983, 1987; Feldman & Laming, 1994; Doschek et al., 2004).

The TR materials are often flowing. By analyzing the spectra obtained by the S082B instrument, Doschek et al. (1976) found that TR lines are often redshifted. The persistent redshifts

of emission lines formed in the middle TR were confirmed in later observations. With SUMER observations, Peter & Judge (1999), Teriaca et al. (1999), Stucki et al. (2000) and Xia et al. (2004) studied the variation of the average Doppler shift with the line formation temperature. They found that the redshift is most significant (~10 km s^{-1}) at ~2×10^5 K and decreases at lower and higher temperatures. Emission lines formed in the lower TR reveal no obvious Doppler shift on average, while emission lines formed in the upper TR are clearly blue shifted. The temperature variation of the TR line shift shows a similar trend in both the quiet Sun and coronal holes. In both regions, the value of the redshift is positively correlated with the line radiance, and is more prominent in the network than in cell interiors (e.g., Curdt et al., 2008a; Aiouaz, 2008). The blue shifts of upper TR lines are predominant in coronal holes and are suggested to be signatures of the fast solar wind (Dammasch et al., 1999; Hassler et al., 1999; Wilhelm et al., 2000; Xia et al., 2003; Tu et al., 2005a; Aiouaz et al., 2005), while blue shifts are localized at network junctions in the upper TR of the quiet Sun (Hassler et al., 1999). In active regions, the redshifts of middle TR lines are about two times larger than those in the quiet Sun (e.g., Teriaca et al., 1999). Different mechanisms such as spicule activities (e.g., Athay, 1984), siphon flows from one loop leg to the other (e.g., McClymont & Craig, 1987; Mariska, 1988), downward propagating MHD waves produced by nano-flares (e.g., Hansteen, 1993; Hansteen et al., 1997) and solar wind related reconnections in the network (Tu et al., 2005a; He et al., 2008) have been suggested to explain these prominent Doppler shifts of TR lines (see reviews and discussions in Mariska, 1992; Brekke et al., 1997; Peter & Judge, 1999; Xia, 2003).

Small-scale transient phenomena such as explosive events, coronal bright points, blinkers and macrospicules are frequently observed in the TR. Explosive events (EEs), which were first identified through HRTS observations (Brueckner & Bartoe , 1983), are characterized by a small spatial scale of about 1800 km, a short lifetime of about 60 s, and non-Gaussian line profiles showing Doppler shifts of ~100 km s^{-1} (e.g., Dere et al., 1989; Innes et al., 1997a; Doyle et al., 2006). EEs tend to occur along boundaries of the magnetic network, where weak mixed-polarity magnetic features are present (e.g., Chae et al., 1998a; Teriaca et al., 2004). They are believed to be produced by magnetic reconnections in the TR (Innes et al., 1997b; Chen & Priest, 2006). Coronal bright points (BPs), which are characterized by locally enhanced emission in X-ray and EUV, are associated with the underlying bipolar magnetic field at network boundaries (e.g. Habbal et al., 1990; Webb et al., 1993; Falconer et al., 1998; Brown et al., 2001; Madjarska et al., 2003; Tian et al., 2007). A BP consists of several miniature dynamic loops (e.g., Sheeley & Golub, 1979; Ugarte-Urra et al., 2004a) and is typically $30'' - 40''$ in size. The average lifetime of BPs is 20 hours in EUV (Zhang et al., 2001) and 8 hours in X-ray observations (Golub et al., 1974). The energization of BPs may be associated with the interaction between two magnetic fragments of opposite polarities (Priest et al., 1994; Parnell et al., 1994), magnetic reconnection along separator field lines (Longcope, 1998), or current sheets induced by photospheric motion (Büchner, 2006; Santos & Büchner, 2007). Blinkers are transient TR network brightenings with a typical duration of 5 to 30 minutes (e.g., Harrison, 1997; Doyle et al., 2004). Macrospicules are jet-like structures extending from the chromosphere into the corona, which could be regarded as the EUV counterpart of the Hα spicules (e.g., Bohlin et al., 1975; Xia et al., 2005).

The hydrogen Lyman lines, especially the Lyα line, play a dominant role in the radiative energy transport in the lower TR (Fontenla et al., 1988). Due to the effect of radiative transfer, a central reversal is usually present in Lyα and Lyβ line profiles. The Lyman line profiles can be used to reveal information on fine structures and physical properties of quiescent prominences (e.g., Heinzel et al., 2005; Vial et al., 2007; Schmieder et al., 2007; Gunár et al., 2008). They can also be used to diagnose nonthermal effects in solar flares (Hénoux et al., 1995; Fang et al., 1995; Xu et al., 2005). Full Lyα and Lyβ line profiles were acquired through early observations more than two decades ago (e.g. Nicolas et al., 1976; Kneer et al., 1981; Lemaire et al., 1978; Vial, 1982; Bocchialini & Vial, 1996; Basri et al., 1979; Fontenla et al., 1988). These observations revealed valuable information on the stratification of the solar upper atmosphere, although the obtained Lyman line profiles were hampered by the geocoronal absorption at the center. The SUMER observations at the first Lagrangian point are free from geocoronal absorptions. By analyzing spectra obtained by SUMER, Warren et al. (1998) found that the average profiles for Lyβ through Lyϵ are all reversed at the center and stronger in the red wing. It has been suggested that the asymmetries of Lyman line profiles are related to the differential flows in the upper solar atmosphere (Gouttebroze et al., 1978; Fontenla et al., 2002; Gunár et al., 2008). Warren et al. (1998) also found larger peak separations of the profiles at limb than at disk center. The full high-quality Lyα line profiles were not recorded on the detectors of SUMER for a long time, because the high radiance of the line usually leads to a saturation of the detector microchannel plates. Attempts have been made to record Lyα on the bare part of detector A. However, the signal determination turned out to be highly uncertain due to the local-gain depression correction (Teriaca et al., 2005a,b, 2006).

Although much has been known about the emission and structures of the TR, there are still many important things that have not or rarely been investigated. For example, almost all studies of the TR network structures are concentrated on the average Sun or quiet Sun (e.g., Gabriel, 1976; Dowdy et al., 1986; Patsourakos et al., 1999; Peter, 2001). But the TR is in fact highly nonuniform (e.g., Marsch et al., 2006) so that differences between different solar regions (quiet Sun, coronal holes, active regions) should be expected. Another aspect is concerning the nature of the flow field in the TR. High-cadence observations reveal that the TR is highly dynamic and transient flows are often detected (e.g., Innes et al., 1997a), while quasi-steady flows lasting from several hours to several days are also observed to be present in the TR (e.g., Marsch et al., 2004; Dammasch et al., 2008). It is hard to imagine how these two kinds of flows could coexist in the TR. Moreover, up-

flows in the upper TR outside coronal holes are not well understood (Hassler et al., 1999; Marsch et al., 2004). The TR above sunspots is also an interesting topic. Although sunspots and plage have been intensively studied in the photosphere and chromosphere (Solanki, 2003), their possible different properties in the TR are not well understood. Finally, the lower TR line Lyα has been suggested to be used in proposed future solar missions such as Solar Orbiter (Marsch et al., 2002), Kuafu (Tu et al., 2008) and SMESE (Vial et al., 2008). Despite its importance, high-quality undisturbed Lyα profiles have not been obtained, and signatures of TR flows and transient phenomena in Lyman line profiles have not been identified in observations before 2008. These open questions are summarized below:

(1) Are there any differences between the TR properties in coronal holes and in the quiet Sun?

(2) Why are quasi-steady flows frequently observed in the TR and corona?

(3) Are there any differences between the TR properties above sunspots and the surrounding plage regions?

(4) What are the characteristics of the origin and initial acceleration of the solar wind in the TR and corona?

(5) What does the genuine solar hydrogen Lyα radiance profile (that unaffected by the atmosphere of the earth) look like?

In the past several years, a lot of work has been done to understand the problems mentioned above. The magnetically structured TR was found to have different properties in different regions through a combination of spectroscopic observations and magnetic field extrapolations. With the help of magnetic field extrapolations, the TR flows in different regions were better explained, and the persistent and transient flows can now be understood in a unified picture. Comprehensive comparisons of TR properties between sunspots and plage regions have also been done in the recent past, and distinct differences were found. A new technique of recording Lyα profiles has been employed by the SUMER team since June 2008, and high-quality Lyα profiles without geocoronal absorption were obtained for the first time. It has been found that TR flows and EEs can modify the observed Lyman line profiles. This article reviews these recent progresses and provides a new view on the TR emission and structures.

2. Quiet Sun

The quiet Sun usually occupies most of the disk area, and thus its properties often represent the average properties of the Sun. Both transient and quasi-steady flows are observed to be present in the quiet-Sun TR.

2.1. Upflows in the upper TR

It is well known that emission lines formed in the middle TR are redshifted by several km s^{-1} on average (e.g., Doschek et al., 1976; Chae et al., 1998c). With increasing temperature, the average redshift of TR lines decreases, and finally turns into blue shift above $\sim 5\times10^5$ K (Peter & Judge, 1999; Teriaca et al., 1999; Stucki et al., 2000; Xia et al., 2004).

Within the SUMER spectral range, the strong Ne VIII 770 Å line formed in the upper TR is of particular value because of its important role in the study of solar wind origin. The average blue shift of this line has been established since 1999, when Dammasch et al. (1999) derived a very accurate rest wavelength of 770.428 ± 0.003 Å for it.

Blue shifts are found almost everywhere on the Dopplergrams of Ne VIII in polar coronal holes (Hassler et al., 1999; Dammasch et al., 1999; Wilhelm et al., 2000). And patches of significant Ne VIII blue shift are also found within equatorial coronal holes (Xia, 2003; Xia et al., 2003; Aiouaz et al., 2005). These blue shifts are usually interpreted as signatures of the nascent fast solar wind, and found to be associated with the chromospheric network (Hassler et al., 1999) where magnetic funnels anchor and expand with height (Tu et al., 2005a).

In the quiet Sun, significant blue shifts of Ne VIII were also found at network junctions and considered to be possible sources of the solar wind (Hassler et al., 1999). However, the magnetic field lines of the quiet Sun are usually closed so that it is difficult to imagine how the materials escape into the interplanetary space.

As a low-β plasma region, the TR should be magnetically structured and the flows of TR plasmas should be largely guided or controlled by the strong magnetic fields. Since currently the magnetic field of the upper solar atmosphere can not be measured directly, magnetic field extrapolation is often adopted by the solar community to study the magnetic coupling of different coronal structures and processes (e.g., Wiegelmann & Neukirch, 2002). The validity of potential-field coronal magnetic field models has been tested and confirmed with recent development of coronal magnetic field measurements (Liu & Lin, 2008). With the assumption that the magnetic field is almost force-free at heights of about 400 km above the photosphere (Metcalf et al., 1995), the force-free model proposed by Seehafer (1978) has been applied successfully in the studies of long-lasting and quasi-steady phenomena and structures in the TR (Marsch et al., 2004; Wiegelmann et al., 2005; Tu et al., 2005a,b; Marsch et al., 2006; Tian et al., 2007; He et al., 2007; Marsch et al., 2008; Tian et al., 2008a,b,c, 2009a).

McIntosh et al. (2007b) mentioned that it is the global magnetic topology that dictates whether the released plasma just provides thermal input to the quiet solar corona or finally feeds the solar wind. In order to investigate the possible source region of the solar wind and the physical meaning of the prominent Ne VIII blue shift in the quiet Sun, He et al. (2007) and Tian et al. (2008a) applied the Seehafer (1978) solution to reconstruct the 3-dimensional (3-D) potential magnetic-field structure in a quiet-Sun region. He et al. (2007) found that a sub-region corresponding to relatively weak emission in the EIT (Extreme ultraviolet imaging telescope) 195 Å image is associated with open field lines. Tian et al. (2008a) further pointed out that these open fields correspond to a magnetic funnel structure in the quiet Sun. Figure 2 shows this structure. It can be seen that the funnel structure consists of two parts: below ~20 Mm, several small funnels originating from different supergranular boundaries expand with height; above ~20 Mm, these small funnels merge into a single wide open-field region. One may speculate that coronal funnel structures

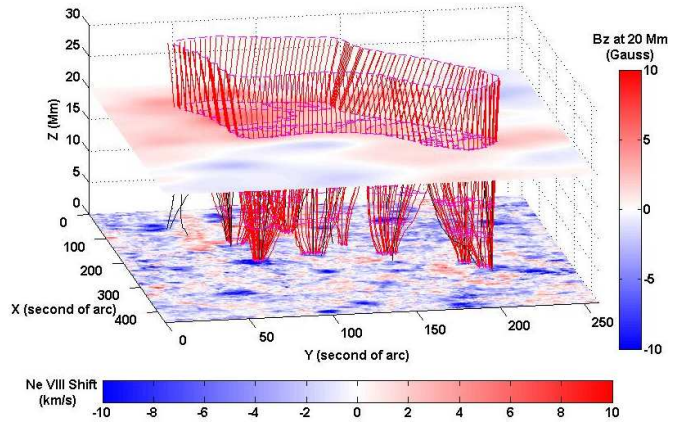

Figure 2: Magnetic funnel structure in a quiet-Sun region. The red lines represent field lines originating from the funnel boundary, and the black ones are open field lines outside the small funnels. The Dopplergram of Ne VIII is placed at the bottom layer. The extrapolated longitudinal field strength at 20 Mm is also shown as a magnetogram placed at the corresponding height. Adapted from Tian et al. (2008a).

in coronal holes should be of a similar form, yet the merging height might be different (Tian et al., 2008b). The existence of the funnel structure, which may result from the local opening of large-scale coronal loops through magnetic reconnections, suggests that the solar wind could also form in the quiet Sun.

However, Figure 2 reveals clearly that most of the patches with significant Ne VIII blue shifts do not coincide with the funnel legs. Thus, as argued by He et al. (2007) and Tian et al. (2008a), these blue-shift sites may not be sources of the solar wind. If the solar wind could actually form in the quiet Sun, it may start at a layer higher than the source region of the Ne VIII emission. If this is the case, significant outflows could perhaps be found in the Dopplergram of another line with a higher formation temperature than that of Ne VIII.

In fact, Tian et al. (2008a) found that the patches with significant blue shift located mainly in network junctions are often associated with legs of large coronal loops. Thus, these blue shifts are more likely to be signatures of mass supply to coronal loops rather than solar wind outflows. The correspondence between the significant blue shift of Ne VIII and loop legs was further investigated by Tian et al. (2009a). It can be seen from Figure 3 that in this quiet-Sun region almost all of the patches with significant blue shift on the dopplergram of Ne VIII coincide with legs of magnetic loops originating from strong-field regions. The loop legs generally exhibit funnel-like shapes, supporting the argument made by Peter (2001) that magnetic funnels can either be connected to the solar wind or form the legs of large coronal loops. Figure 3 also reveals that some blue-shift patches are even associated with the common leg of several joint loops with different spatial scales and orientations. Thus, the mass and energy flowing into a single funnel can then be spread and supplied to multiple loops.

Under the assumption that the Doppler shift of Ne VIII can be used as a proxy for the plasma bulk flow (i.e., of the proton flow) (Xia et al., 2003; Marsch et al., 2004), Tian et al. (2009a) calculated the rate of mass supply to coronal loops for each

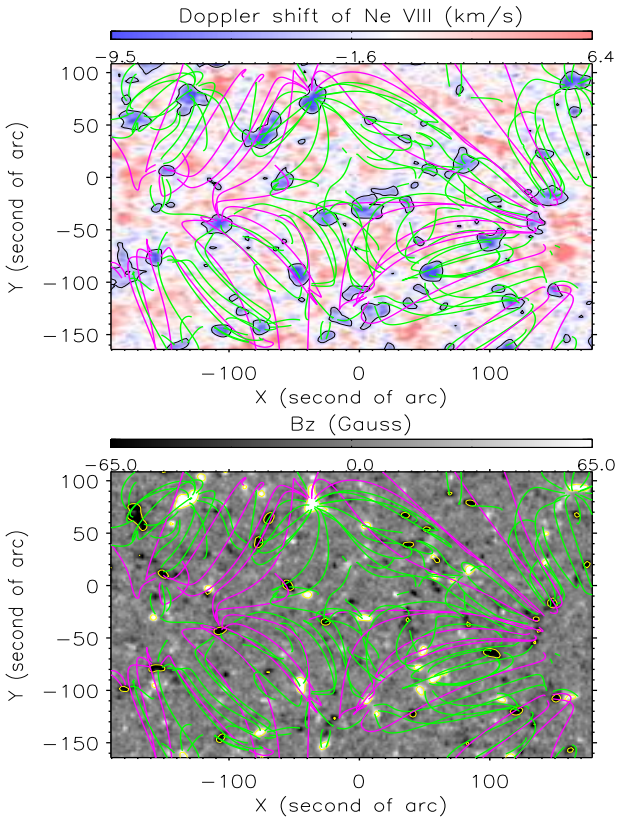

Figure 3: Projections onto the x-y plane of the extrapolated magnetic field lines, being superposed on the maps of the Doppler shift of Ne VIII (upper panel) and the photospheric longitudinal magnetogram (lower panel), in a quiet-Sun region. Field lines reaching higher and lower than 40 Mm are plotted in purple and green, respectively. Contours in the two panels outline regions with significant blue shift of Ne VIII and those with strong magnetic field, respectively. Adapted from Tian et al. (2009a).

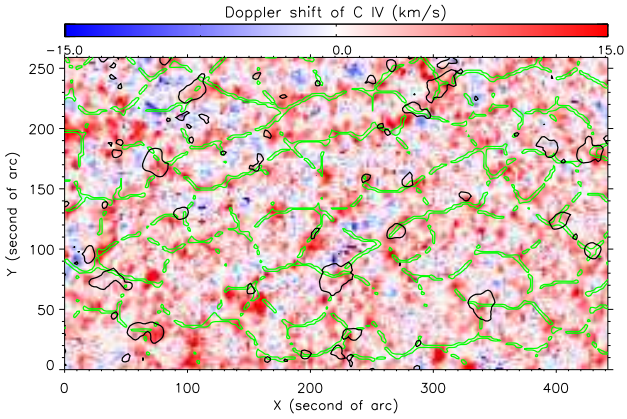

Figure 4: The contours outlining the most significant blue shift of Ne VIII are superposed on a Dopplergram of C IV. The pattern of the chromospheric network is shown in green. Adapted from Tian et al. (2010b).

funnel-like loop leg. They found an anti-correlation between the mass flux and the expansion factor of the loop leg from the photosphere to 4 Mm (formation height of Ne VIII, Tu et al., 2005b) above the photosphere. It is known that the expansion rate of the large-scale magnetic field structures largely determines the speed of the solar wind (e.g., Wang et al., 1990; Wang, 2009). Tian et al. (2009a) argued that the expansion rate of the loop leg could possibly be related to the observed mass flux. In a strongly diverging funnel-like loop leg, most of the energy that is brought in by the cool plasma and produced in heating processes may be deposited in the lower layer of the loop leg (below the formation height of Ne VIII), and therefore the energy used to drive the upflow in the upper TR will be reduced. In contrast, if the expansion of the loop leg is weak, more energy will be used to accelerate the upflow, and thus the upward mass flux will be increased.

2.2. Transient and quasi-steady flows in the TR

Transient flows lasting from several seconds to several minutes are often detected in the TR. For example, transient siphon flows have been observed to be present along small-scale cold loops in the quiet Sun (Teriaca et al., 2004; Tian et al., 2009a). The transient siphon flow reported by Tian et al. (2009a) occurred in a weak mixed-polarity field region located outside the adjacent funnel-like loop leg. Thus, it should not be related to the long-lasting upflow in the loop leg. In the TR structure proposed by Peter (2001), siphon flow is the dominant type of flow in coronal loops. However, observations seem to suggest that siphon flows rarely exist in quiet-Sun coronal loops with sizes comparable to or larger than supergranules. Thus, the dominant flows at upper-TR temperatures in quiet-Sun coronal loops are the long-lasting upflows rather than siphon flows (Tian et al., 2009a).

Both the downflows in the middle TR and upflows in the upper TR are almost steady on the time scale of one day, comparable to the life time of the network. Figure 4 illustrates the spatial relationship between prominent redshifts of a middle TR line C IV and patches of the most significant blue shift of Ne VIII. The figure reveals clearly that the redshifts of C IV are usually very strong along the network, and that prominent blue shifts of Ne VIII are concentrated in network junctions where several cells converge. As pointed out by Tian et al. (2010b), the locations of strong upflows in the upper TR are often cospatial with strong downflows in the middle TR. However, in some cases the prominent blue shifts of Ne VIII do not fully coincide with but slightly deviate from the strongest red shifts of C IV, which might be related to the height variation of the network magnetic field (Aiouaz, 2008; Tian et al., 2008e).

The relationship between the persistent redshifts of cool lines and blue shifts of lines formed at higher temperatures is not well understood. In coronal holes, the blue and redshifts were explained by Tu et al. (2005a) and He et al. (2008) as the upflow and downflow after magnetic reconnection between open field lines in coronal funnels and cool loops on the sides. In the quiet Sun, magnetic reconnections might also occur if the magnetic polarities of side loops are opposite to those of funnel-like loop legs. Thus, the scenario of continuous magnetic reconnection might also be the mechanism responsible for the bidirectional flows in the TR, (Aiouaz, 2008; Tian et al., 2008a, 2009a). Aiouaz (2008) proposed a TR structure which involves reconnections between the strong network magnetic field and continuously advected weak field from the supergranular cell interior for both the quiet Sun and coronal holes. The resulting downflows and upflows are then observed to be the redshifts of emission lines formed in the middle TR and the blue shifts of upper-TR lines, respectively.

As an alternative explanation, the redshifts of middle-TR lines might also correspond to the downward cooling plasma after the velocity of the upflows decreases to zero. As mentioned by Tian et al. (2009a), cool photospheric and chromospheric plasmas can continuously enter loop legs through processes such as magnetic reconnection and diffusion from outside. These plasmas may then flow up and speed up along the loop legs when the heating is switched on, leading to significant blue shifts of lines formed in the upper TR. Due to the onset of possible (radiative) cooling effects, the flows might decelerate above a certain height (perhaps in the lower corona) and finally turn downwards and accelerate under gravity, leading to emission by the dense plasma at lower temperatures and causing the redshifts of middle-TR lines. The steadiness of the observed shifts suggests that all these processes should occur continuously and persistently.

Occasionally, part of the large-scale quiet-Sun coronal loops could locally be opened through processes such as magnetic reconnection. Due to the decrease of the magnetic tension, the upflowing materials might speed up and reach higher layers along the magnetic field lines, and could finally be released into the solar wind after further acceleration.

Based on many observations of long-lasting flows in the TR and corona, Marsch et al. (2008) proposed the concept of "coronal circulation", or "coronal convection", to emphasize that the plasma in the TR and corona is flowing all the time, leading to quasi-steady average flows which are strongly guided by the dominant magnetic field. In fact, a similar idea was suggested more than three decades ago by Foukal (1978). The quasi-

steady flow field can be regarded as the background flow field in the TR and corona. While occasionally small-scale transient flows could locally occur and superpose on the background field.

2.3. Flow field of coronal bright points

Coronal bright points are small-scale bipolar features indicating local heating in the TR and lower corona. It is believed that a BP consists of several miniature loops (e.g., Sheeley & Golub, 1979; Ugarte-Urra et al., 2004a), and that the emission of a BP is usually highly dynamic (e.g., Habbal et al., 1990; Ugarte-Urra et al., 2004a,b).

The relationship between the dynamic emission of BPs and the evolution of the underlying photospheric magnetic field has been intensively studied (e.g., Brown et al., 2001; Madjarska et al., 2003). While the plasma diagnostics as well as the flow field of BPs have only been investigated recently. The electron density of BPs, which is vital to determine the radiative losses in models of coronal heating, was derived at coronal temperatures (Ugarte-Urra et al., 2005; Brosius et al., 2008; Tian et al., 2008d; Dere, 2008, 2009; Doschek et al., 2010) and TR temperatures (Tian et al., 2008d) in the last several years. The differential emission measure (DEM) of BPs was found to peak around $\log(T/\mathrm{K}) = 6.15$ (Brosius et al., 2008; Doschek et al., 2010). Dere (2008) and Dere (2009) determined the volumetric plasma filling factor of BPs, which varies from 4×10^{-5} to 0.3.

The flow field of BPs has rarely been investigated. Madjarska et al. (2003) noticed that the Doppler shift of S VI in a BP is in the range of -10 to 10 km s^{-1}. Xia et al. (2003) reported small blue shift of Ne VIII associated with BPs in an equatorial coronal hole and concluded that BPs are not directly related to the solar wind outflow. Through an analysis of the spectroscopic data obtained by the Extreme Ultraviolet Normal Incidence Spectrograph (EUNIS) sounding rocket instrument, both strong upflow and downflow in a BP were found by Brosius et al. (2007). In that observation, Doppler shifts on opposite sides of a BP were found to be about ± 15 km s^{-1} in emission lines formed in the TR and up to ± 35 km s^{-1} in coronal lines. These bi-directional high-speed flows were interpreted to be the result of magnetic reconnections, which is possible since magnetic reconnections are involved in most proposed energization mechanisms of BPs (e.g., Priest et al., 1994; Longcope, 1998; Büchner, 2006).

The observation made by Brosius et al. (2007) could only provide the distribution of Doppler shift along the slit. Two-dimensional (2-D) flow field of a BP was investigated by Tian et al. (2008d). In a coordinated observation of SUMER and EIS, 12 EUV lines with formation temperatures from $\log(T/\mathrm{K}) = 4.5$ to 6.3 were used to derive the 2-D flow field of the BP at different temperatures. Figure 5 shows the spatial distribution of the Doppler shift of each line. Patches of red and blue shift are both found in the BP with comparable sizes. The absolute shift is largest in middle-TR lines ($\log(T/\mathrm{K}) = 4.9 - 5.2$) and can reach more than 10 km s^{-1}. The figure also reveals clearly that the Doppler shifts in the BP are quite different in different lines, e.g., the boundary between up/down flows in the BP is almost perpendicular at lower and higher temperatures, with the transition occurring at a temperature of about $\log(T/\mathrm{K}) = 5.7$. This temperature-dependent Doppler shift in the BP might be the result of a syphon flow along the associated loop system which twists or spirals at its upper segment. Considerable magnetic helicity seems to be present in such a loop system.

The different Doppler-shift pattern of the BP at lower and higher temperatures may also imply a different powering mechanism of the BP at different heights. McIntosh (2007a) proposed a two-stage heating mechanism of BPs, in which magnetoconvection-driven reconnection occurs in, and supplies energy to, the relatively cool component of the BPs. The increased energy supply then leads to an expansion of the associated loop system, which interacts with the overlying coronal magnetic field through fast separator reconnection and produces hot plasmas of the BPs. Signatures of magnetic flux cancelation and separator reconnection were indeed found by Tian et al. (2008d), thus favoring the two-stage powering mechanism mentioned above.

In fact, significant downflows and upflows on opposite sides of BPs are found not only in the quiet Sun (Brosius et al., 2007; Tian et al., 2008d), but also in coronal holes (Tian et al., 2010a). This kind of flow field seems to be common for BPs in both regions. There are also some BPs revealing blue shifts of upper-TR lines in both legs of the associated loop system (Tian et al., 2009a, 2010b). These BPs are usually associated with relatively large-scale magnetic loop systems, and thus have a flow pattern similar to those of large-scale coronal loops in the quiet Sun.

From Figure 5 it is also clear that the TR flow fields of the BP at different times could have a similar pattern, which indicates the steadiness of the flows on a time scale of $\sim$2 hours. Thus, the flow field of the BPs also has a quasi-steady component, although the emission of the BPs is believed to be highly dynamic and fluctuating.

2.4. Lyman line radiances and profiles in the quiet Sun

Hydrogen is the most abundant element in the solar atmosphere and its resonance lines, especially the Lyα line, play a key role in the overall energy transport in the solar atmosphere. The Lyα line is in fact the strongest emission line in the FUV/EUV spectral range and the energy loss through its emission is the most important radiative loss in the lower TR (Fontenla et al., 1988).

SUMER observations of the hydrogen Lyman lines have several advantages over observations made by earlier instruments. First, SUMER observations at the L1 point do not have the problem of geocoronal absorption. Second, the spectral range of SUMER covers the whole hydrogen Lyman series as well as the Lyman continuum (Curdt et al., 2001). Third, SUMER observations can provide full Lyman line profiles in very high spatial, temporal, and spectral resolutions (Wilhelm et al., 1995; Lemaire et al., 1997).

A complete description of the radiances and profiles of higher Lyman series lines (from Lyβ to Lyλ; $n = 2, \cdots, 11$) was

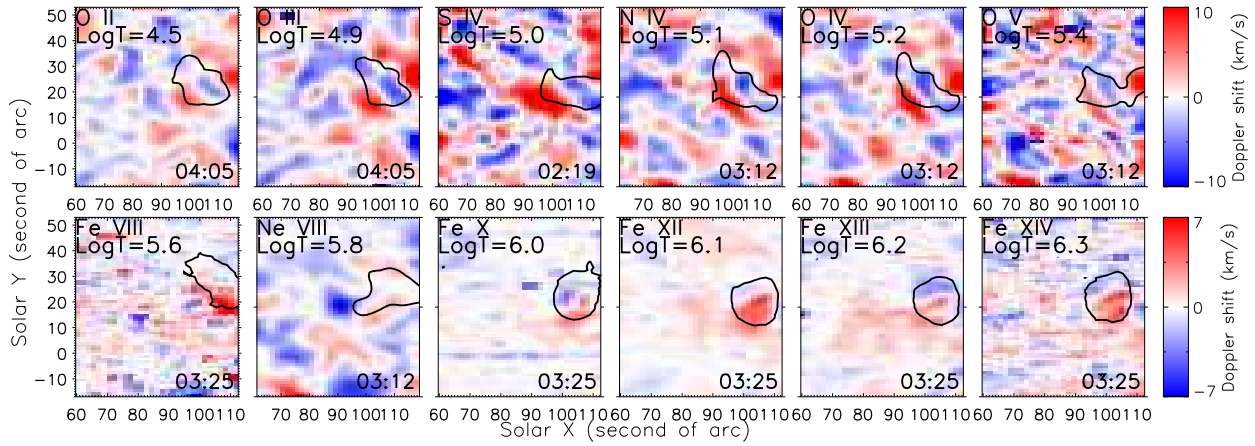

Figure 5: Flow field of a coronal bright point (BP) at different temperatures. The approximate time when the BP was scanned is shown in the lower right corner of each dopplergram. The black contours outline the positions of the BP as seen in emission lines. Adapted from Tian et al. (2008d).

presented by Warren et al. (1998). They found that: (1) the average quiet-Sun profiles for Lyβ through Lyϵ are self-reversed, and the remaining lines are flat-topped; (2) the network profiles show a strong enhancement in the red wings, while the internetwork profiles are nearly symmetric; (3) the radiative transfer effect is much more significant at the limb than at disk center; (4) the Lyman-line limb brightening is weak compared to that of optically thin TR emission lines.

Higher order Lyman lines (from Lyϵ to Lyλ) obtained above the polar limb were found to be nearly Gaussian, and thus could be used to diagnose the variation of the hydrogen temperature with height in the solar atmosphere (Marsch et al., 1999, 2000). The authors found that the line width of the Lyman lines increases with decreasing main quantum number. They also found that the hydrogen temperature only slightly increases from $\sim 1\times10^5$ K at the height of 12 Mm to $\sim 2\times10^5$ K at 18 Mm. It was concluded that the temperature gradient of the TR is very small and does not reveal a steep jump expected from models of the solar atmosphere (e.g., Vernazza et al., 1981). The smooth temperature change across the TR was suggested to be the result of a mixing of various sub-structures in which the abrupt temperature jumps are located at different heights (Marsch et al., 2000).

Since the enormous radiance of the Lyα line could lead to a saturation of the detector microchannel plates, high-quality full Lyα profiles without geocoronal absorption had not been acquired by SUMER before 2008. In June 2008, the SUMER team began to use an unconventional method, partly closing the aperture door to reduce the incoming photon flux by ~80%, and obtained high-quality undisturbed Lyα profiles for the first time. Spectra of a typical middle-TR line Si III 1206 Å was also obtained quasi-simultaneously. As an unexpected result, most Lyα profiles are strongly reversed and have a stronger blue peak (Curdt et al., 2008b; Tian et al., 2009d). This asymmetry is opposite to those of most Lyβ profiles. Moreover, the profile is almost symmetric when the Doppler shift is small, while the profile asymmetry becomes stronger with the enhancement of the downflow in the middle TR.

Gouttebroze et al. (1978) suggested that the asymmetries of

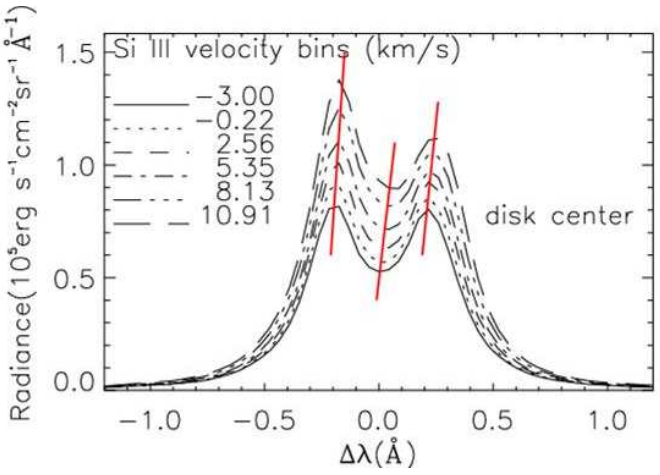

Figure 6: Lyα profiles in Si III-Doppler-shift bins, with the levels of Doppler shift marked in the figure. With increasing red shift of Si III, positions of the Lyα line peaks and central depression are offset towards longer wavelengths, as indicated by the red tracing lines. Adapted from Curdt et al. (2008b).

Lyman line profiles are probably related to large-scale motions of the solar atmosphere. Fontenla et al. (2002) and Gunár et al. (2008) further concluded through numerical simulations that plasma motions could indeed modify the Lyman line asymmetries. Results presented in Curdt et al. (2008b) and Tian et al. (2009d), which demonstrated that the TR flows play an important role in shaping the Lyα profiles, are the first observational evidence of the close relationship between plasma motions and Lyman line profile asymmetries. One could assume that the profiles of the Lyα radiation from the upper chromosphere and lower TR are nearly symmetric (Fontenla et al., 1988). When the Lyα emission goes upwards through the middle TR, the red wings (mainly between the line center and the red peak) of the Lyα profiles will be absorbed by the hydrogen atoms in the downflowing plasma. With the enhancement of the downflow, the spectral position where the absorption is strongest moves towards the red peak, leading to a weakening of the red peak and a strong asymmetry of the profiles. The red tracing lines in

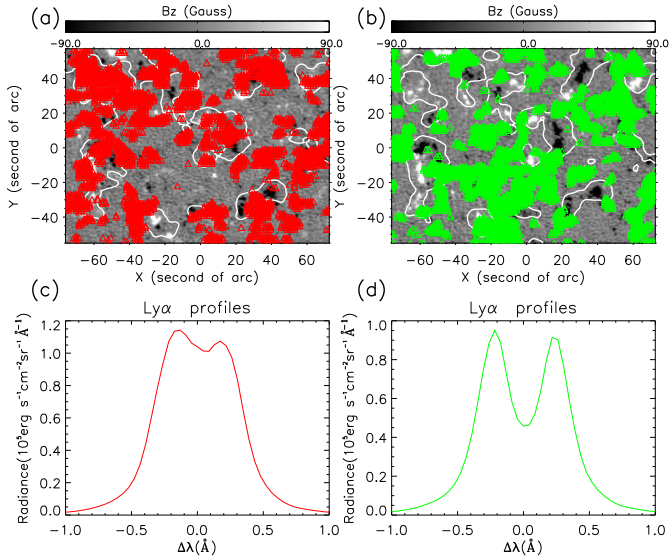

Figure 7: Spatial distribution of Lyα profiles with different self-reversal depths. Positions of Lyα profiles having the most shallow (a) or deepest (b) self-reversals are marked by triangles on the grey-scale MDI magnetogram. The white contours outline the network pattern on the corresponding Lyα radiance image. The averaged Lyα profiles at positions marked in (a) and (b) are shown in panels (c) and (d), respectively. Adapted from Tian et al. (2009d).

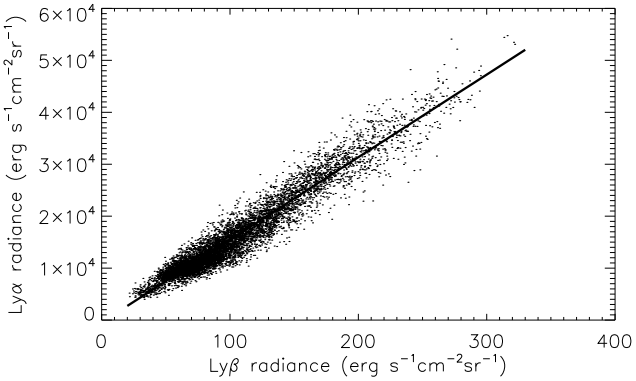

Figure 8: Relationship between the radiances of Lyα and Lyβ in the quiet Sun. The straight line shows the linear fit to the scattered data points.

Figure 6 clearly show this trend.

The spatial distribution of Lyα profiles with different self-reversal depths was studied by Tian et al. (2009d). From Figure 7 it is clear that locations of the profiles with shallow self-reversals tend to cluster in and around the network, while strongly reversed profiles are often observed in internetwork regions. These different tendencies may result from the different magnetic structures between the two regions. In the network, magnetic loops of different sizes and funnels are omnipresent in the chromosphere and TR. The Lyα emission originates from the outskirts of these structures, experiencing a relatively weak radiative transfer. In contrast, in the cell interiors, only low-lying cool loops are present and the Lyα emission sources are mainly located at a much lower height compared to the network. Thus, in the internetwork region the opacity is enhanced and the Lyα radiation penetrating the upper layers will be absorbed more strongly.

The Lyα profiles in quiescent prominences, which were found to be only slightly self-reversed, were presented by Curdt et al. (2010). They also found that the Lyα profile is more reversed when seen across the magnetic field lines (prominence axes) than along the field lines, consistent with the prediction made by Heinzel et al. (2005) and complementing a similar finding for higher order Lyman lines (Schmieder et al., 2007).

The Lyα/Lyβ radiance ratio is also of great interest since it is very sensitive to the local physical and geometrical properties of many solar structures such as the quiescent prominence (Vial et al., 2007). Calculations by Gouttebroze et al. (1993) suggested a value between 90 and 400 for this ratio (energy unit). However, early observations made by Skylab and OSO 8 yielded a value of only 35-90 (Vernazza & Reeves, 1978; Lemaire et al., 1978; Vial, 1982). These low values of the ratio might be problematic due to the relatively low measurement accuracy of the instruments and the error induced by the correction of the geocoronal absorption. The error of the radiometric calibration is only 15%-20% for most emission lines in SUMER observations (Wilhelm et al., 1998). By collecting the scattered light, Lemaire et al. (2005) reconstructed the full-disk Lyα and Lyβ profiles through SUMER observations and obtained a value of about 130 for the ratio. The median value of the Lyα/Lyβ ratios in two recent quiet-Sun observations of SUMER was found to be 160 and 190, respectively (Curdt et al., 2008b; Tian et al., 2009d). So the SUMER observations are consistent with the prediction of Gouttebroze et al. (1993). Figure 8 further reveals that the radiance of Lyα is highly correlated with that of Lyβ in the quiet Sun.

Possible signatures of TR dynamic events in Lyman line profiles have been investigated by Madjarska & Doyle (2002) and Zhang et al. (2010). Madjarska & Doyle (2002) found that profiles through Lyζ to Lyλ reveal central depressions during EEs. The authors suggested that an emission increase in the wings of the Lyman line profiles might be responsible for the observed central depressions. A recent study of searching for signatures of EEs in Lyβ profiles has been performed by Zhang et al. (2010), who found that the central parts of the Lyβ profiles are obviously more reversed and the distance of the two peaks increases during EEs. The authors suggested that the bi-directional jets produced by EEs emit Doppler-shifted Lyβ photons and cause enhanced emission at the positions of the Lyβ profile peaks.

At the end of this section, we have to mention that here we only considered the impacts of TR structures, flows, and dynamic events on the Lyman line profiles. In fact, many factors such as the temperature, density, and flows in different layers of the upper solar atmosphere could all influence the production and propagation of the Lyman line emission. The roles of the density and temperature in shaping the Lyman line profiles are difficult to investigate with the current observations, and they should be considered in future models including calculations of non-LTE (local thermodynamic equilibrium) radiative transfer.

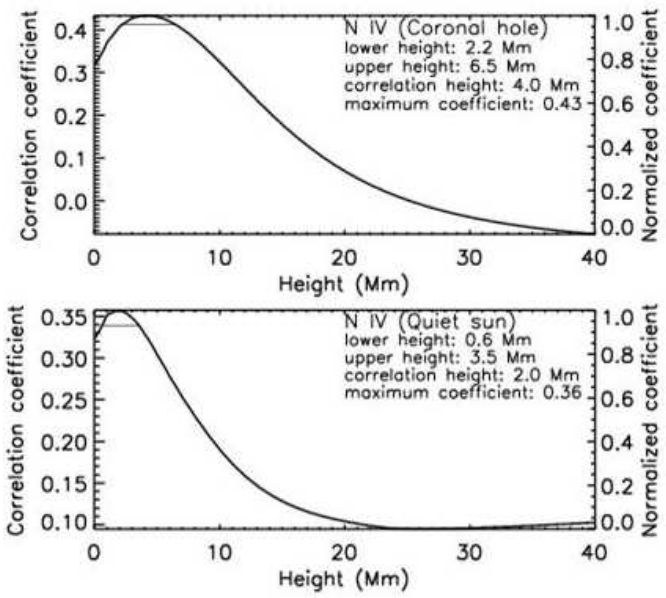

Figure 9: Height variation of the correlation coefficient between the radiance of N IV and $|B_z|$, for a coronal hole (upper panel) and a quiet-Sun region (lower panel). The horizontal bar in each panel shows the height range in which the coefficient is above 95% of the maximum. Adapted from Tian et al. (2008c).

3. Coronal holes

The TR is a highly nonuniform layer, and the magnetic structures and plasma distributions are largely different in coronal holes and in the quiet Sun. In this section, recent progress in comparative studies of the TR properties between the two regions, as well as the spectroscopic observations of the initial acceleration of the fast solar wind in coronal holes, are reviewed.

3.1. Spatial extension of the TR

In classical models of the solar atmosphere (e.g., Vernazza et al., 1981), the TR is described as a thin layer, with a height of about 500 km. The scenario of a thin TR might be true in local regions. For instance, when making the assumption that the height where the radiance of an EUV/FUV emission line maximizes above the limb can be regarded as the main source region of the line, we can expect the various TR lines with different formation temperatures to be emitted from approximately the same height, thus indicating the existence of a very thin TR (Mariska, 1992). However, the TR is in fact highly nonuniform in horizontal directions so that the spatial extension (in the radial direction) of the TR is likely to be different in various regions.

In order to determine the formation heights of emission lines in disk observations, Tu et al. (2005b) invented the method of correlation height analysis. First the force-free solution of Seehafer (1978) was used to calculate the magnetic field vector at every grid point inside a cubic volume. The correlation coefficient between the 2-D distribution of the line radiance (usually for emission lines formed in the lower and middle TR) or the Doppler shift (usually for emission lines formed in the upper TR), and the 2-D distribution of the vertical component of the extrapolated magnetic field, was calculated at each height. Then the concept of emission height was introduced, which was assigned to the height at which the correlation coefficient reaches its maximum (see Figure 9). The correlation height could be regarded as a rough estimate of the real height of the emission source, or some kind of average emission height if the emission source is widely spread in height. As mentioned in Marsch et al. (2006), in the low-β TR region, with the magnetic field being frozen into the plasma flow, the 2-D (horizontal) density distribution and vertical motion of the emitting ions should be largely controlled by the vertical component of the magnetic field at the line emission height. Thus, a correlation of the two should be expected, and the height at which their correlation maximizes should approximately represent the real height of the emission source. A possible correlation between the magnetic field and plasma density (expressed as the square root of a line radiance as a first order approximation) may also be expected from the theoretical point of view that the heating energy flux (being proportional to the density) entering loops is proportional to the magnetic field strength (Schrijver, 2004).

Tu et al. (2005a) applied the method of correlation analysis mentioned above to a polar coronal hole. They found a correlation height of ~20 Mm for the upper-TR line Ne VIII, and 4-5 Mm for the lower-TR line Si II and middle-TR line C IV. Based on this result, Tu et al. (2005a) concluded that the nascent fast solar wind originates at a height range between 5 and 20 Mm in magnetic funnels. The correlation heights of the same emission lines were determined in a high-latitude quiet-Sun region by Tu et al. (2005b), who found a correlation height of ~4 Mm for Ne VIII and ~2 Mm for the other two lines. Marsch et al. (2006) determined the correlation heights of 12 emission lines with formation temperatures ranging from 7.4×10^3 K to 3.0×10^5 K in a polar coronal hole. They found a correlation height of 2-3 Mm for these lines in a bright subregion, and 9-12 Mm in a weak-emission subregion. This result suggests that the TR is highly structured and plasma at different temperatures can coexist locally at almost the same height in the TR.

The ambiguity caused by the projection effect usually can not be neglected in high-latitude observations. Thus, it would be necessary to check if the same results can be obtained at disk center. The method of correlation analysis was applied by Tian et al. (2008c) to a low-latitude region consisting of an equatorial coronal hole and the surrounding quiet Sun. The result was summarized in Figure 10. The emission heights of all the middle-TR lines were found to be very close in either the coronal hole or the quiet-Sun region, confirming the conclusion that plasma at different temperatures can coexist locally at almost the same height in the TR (Marsch et al., 2006). In the coronal hole, the correlation heights of the middle-TR lines are 4-5 Mm, while in the quiet-Sun region the heights are around 2 Mm, indicating a higher location of the TR in the coronal hole. The correlation height of the upper-TR line Ne VIII is even more different in both regions. In the quiet Sun, it is similar to those of the middle-TR lines. While the correlation height of Ne VIII in the coronal hole is 9.8 Mm, which is systematically

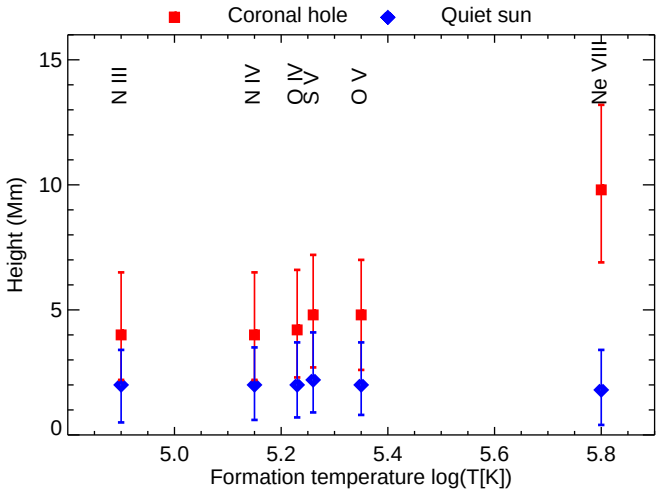

Figure 10: Correlation heights for emission lines formed at different temperatures, in both the quiet Sun and coronal hole. The squares and diamonds represent the correlation heights and the bars indicate the height ranges in which the coefficients are above 95% of the maxima. Adapted from Tian et al. (2008c).

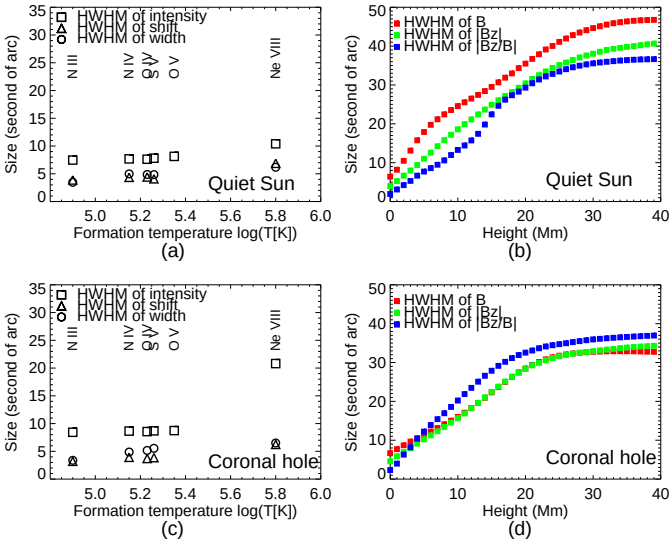

Figure 11: Temperature/Height variations of the characteristic sizes of features in images of intensity, Doppler shift and non-thermal width (left), as well as of the extrapolated magnetic field (right) in the quiet Sun and coronal hole. Adapted from Tian et al. (2008b).

higher than that of a middle-TR line. With the assumption that the difference between the correlation height of a middle-TR line and that of an upper-TR line approximately represents the thickness of the TR, it is clear from Figure 10 that the TR is much thicker, or more extended in altitude, in the coronal hole than in the quiet Sun.

3.2. Expansion of network structures

In the chromosphere most of the magnetic fluxes are concentrated in the supergranular boundaries. The magnetic field structures expand with height through the TR, leading to a much more uniform corona (e.g., Gabriel, 1976). The bright network emission of the TR is associated with the strong magnetic field.

The variation of the network size with temperature was investigated by Patsourakos et al. (1999) through a Fourier-based two-dimensional autocorrelation technique. They first calculated the 2-D autocorrelation function (ACF) of each TR radiance image (obtained with the CDS instrument) by shifting it in both spatial dimensions, and then took its angular average in rings of integer radius and derived a curve of the correlation coefficient against radial distance. The HWHM of the ACF was used to determine the network size. A sharper central peak of the ACF generally corresponds to a smaller size of the bright feature. By using this method, Patsourakos et al. (1999) found that the network size is almost constant from $\log(T/\mathrm{K}) = 4.5$ to $\log(T/\mathrm{K}) = 5.4$, but increases dramatically above $\log(T/\mathrm{K}) = 5.6$. They compared the observed temperature variation of the network size with the expansion of the network width predicted by the model of Gabriel (1976), and found a reasonable agreement.

Gontikakis et al. (2003) further studied the sizes of structures in images of Doppler shift and line width, but only for three lines in a quiet-Sun region. They found that the size of bright radiance features is always larger than that of structures in the maps of the Doppler shift and line width, and attributed it to the fact that the observed Doppler shift and non-thermal motion correspond to the line-of-sight components, which are usually more prominent in loop legs than at loop apex.

Ravindra & Venkatakrishnan (2003) also used the autocorrelation technique, as well as the so-called structure function, to study the life time and length scale of the TR network cells seen in the He II (304 Å) filtergrams obtained by the Extreme-ultraviolet Imaging Telescope (EIT). The magnetic network was also studied by applying their methods to the extrapolated magnetic field at different heights. They found that the magnetic network element equals the size of the He II network element at a height of 3 Mm above the photosphere.

The possible difference between the expansion of TR structures in coronal holes and the quiet Sun was investigated by Tian et al. (2008b). They calculated the ACF for each image of intensity, Doppler shift, and non-thermal width of EUV lines obtained by SUMER, as well as the corresponding extrapolated magnetic field at different heights. Similar to Patsourakos et al. (1999), the HWHM of the ACF was considered to be the characteristic size of the feature. As noticed by Gontikakis et al. (2003), a larger size of the radiance feature in comparison to those of the Doppler shift and non-thermal with was also found at all temperatures. Figure 11 shows that the sizes of all the three features are rather constant for lines with different formation temperatures formed in the middle TR. But in the upper TR, there clearly is a different behavior between the coronal hole and the quiet Sun. Although the sizes of the Ne VIII structures are larger than those present in the middle TR, in both the coronal hole and quiet Sun, the increase in the size of the radiance feature from the middle to the upper TR is apparently much larger in the coronal hole. This indicates that the TR network expands much more strongly with height in the coronal hole than in the quiet-Sun region.

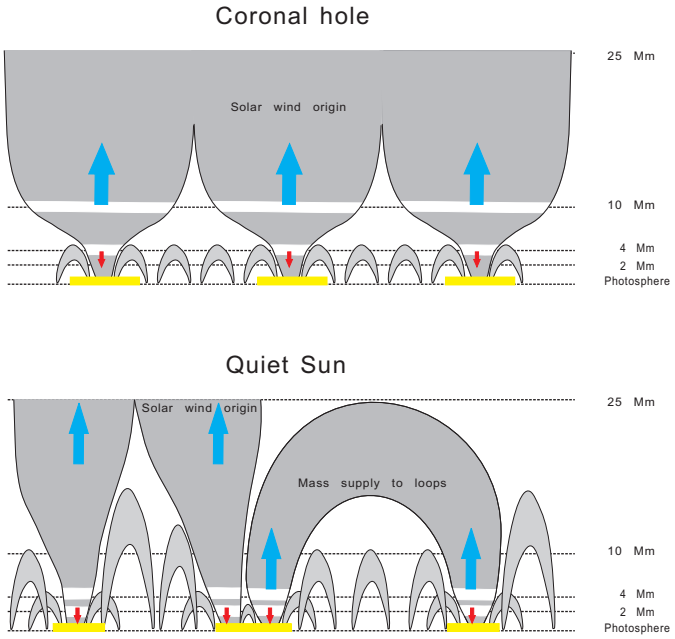

Figure 12: Schematic representation of the magnetic structures in coronal holes (upper panel) and quiet Sun (lower panel). The two white bars in each funnel or loop leg indicate the spatial extension of the TR. Blue and red arrows represent upflows and downflows, respectively. The locations of the network are indicated by the yellow bars. Adapted from Tian et al. (2010b).

The height variation of the sizes of the extrapolated magnetic field parameters B, $|B_z|$ and $|B_z/B|$ was also investigated by Tian et al. (2008b). Figure 11 reveals that the HWHM of $|B_z|$ and B increase linearly with height in the lower layer of the coronal hole. The sizes (in terms of HWHM) of the two features are equal to each other at 10 Mm, implying that small loops only reside below 10 Mm, and that the magnetic field is entirely open above 10 Mm. This result is consistent with the previous conclusion that high loops rarely exist in coronal holes (Wiegelmann & Solanki, 2004; Zhang et al., 2006). While the curve of the HWHM of $|B_z|$ is always lower than that of B, indicating the presence of magnetic loops with different heights up to 40 Mm in the quiet-Sun region. The height variation of the size of $|B_z/B|$ can provide information on the expansion of magnetic structures. Tian et al. (2008b) found that below 10 Mm the size of $|B_z/B|$ increases strongly with height, which indicates a much larger expansion of the magnetic field structures in the coronal hole than in the quiet Sun.

As mentioned in the introduction, TR structures consisting of various types of magnetic features have been proposed by Dowdy et al. (1986) and Peter (2001). However, these studies only concentrated on the quiet or average Sun, and did not point out the possible differences between coronal holes and the quiet Sun. Based on several recent observations (Tu et al., 2005a,b; Tian et al., 2008a,b,c, 2009a; He et al., 2007, 2009), Tian et al. (2010b) proposed a new sketch of the TR structure, with obvious differences between the coronal hole and quiet Sun (see Figure 12). The TR has a height extension of approximately 4-10 Mm in coronal holes and only 2-4 Mm in the quiet Sun. In coronal holes, open magnetic funnels guiding the fast solar

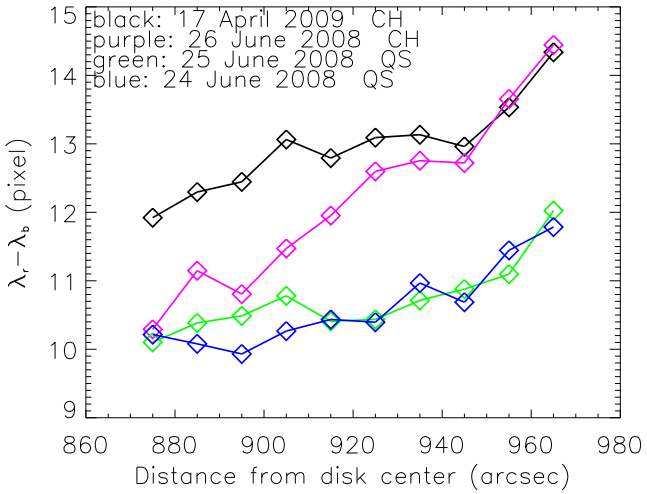

Figure 13: The variation of the peak separation of the Lyα profile with the distance from disk center. Adapted from Tian et al. (2009b).

wind are the dominant magnetic structures. Most of the magnetic loops reside only in the lower part of the atmosphere, and large-scale loops are rarely present. Thus, in coronal holes magnetic funnels can expand strongly in the TR. In the quiet Sun, magnetic loops with different sizes are crowded, which only permits a weak expansion of the legs of large loops and possible open funnels. Upflows in the network of these local open-field regions can possibly work their way up to higher layers, finally merge and form the solar wind.

3.3. Lyman line emission from coronal holes

Although it is well known that the Lyman line emission is obviously reduced in coronal holes compared to the quiet Sun, the coronal-hole Lyman line profiles have rarely been investigated through observations. Xia (2003) noticed that the red peak of the average Lyβ profile in equatorial coronal holes is stronger than the blue peak, which is similar to that in the quiet Sun. However, he found a weaker profile asymmetry and more profiles with blue-peak dominance in coronal holes than in quiet-Sun regions.

Lyα profiles in coronal holes were recently obtained through SUMER observations (Tian et al., 2009b). Figure 13 demonstrates that in both coronal holes and quiet-Sun regions the peak separation of the Lyα profile increases towards the limb, which might be due to the enhancement of the radiative transfer effect resulting from the longer integration path in the line-of-sight direction at the limb. This result complements the previous finding by Warren et al. (1998) for Lyβ through Lyϵ. Tian et al. (2009b) also found a larger peak separation of the Lyα profile which is indicative of a larger opacity in coronal holes than in the quiet Sun. Note that the small values of the peak separation at small distances (further away from the pole) are due to a contamination of some quiet-Sun structures at the boundary of the coronal-hole region scanned on 26 June 2008. Tian et al. (2009b) argued that the nearly perpendicular orientations between the line of sight and the magnetic field lines, and/or a weaker ionizing radiation field in the upper TR and corona,

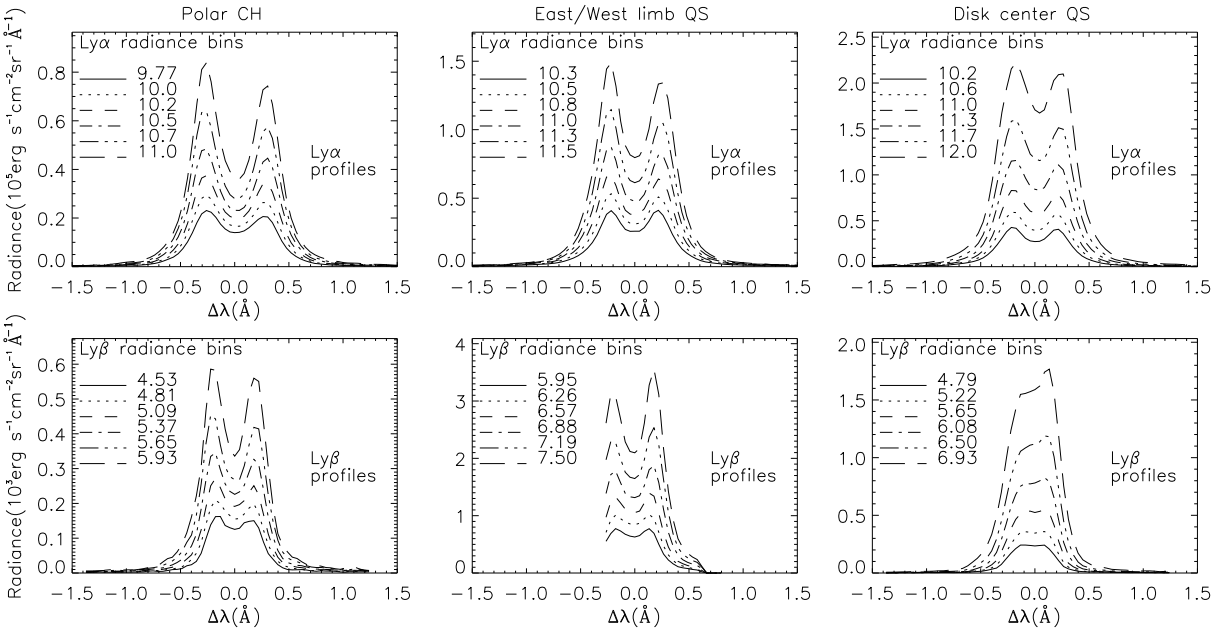

Figure 14: Averaged Lyα (upper panels) and Lyβ (lower panels) profiles in six different radiance bins, as obtained from different locations of the Sun. The levels of the bins are also shown in each panel. Adapted from Tian et al. (2009b).

might be responsible for the larger opacity in coronal holes. In the latter case, the reduced radiative ionization leads to more atomic hydrogen in the upper TR and corona, causing a stronger absorption of the profiles.

The asymmetry of the Lyα profiles is not so different in coronal holes and in the quiet Sun. While this is not the case for the Lyβ line which has a much smaller opacity compared to Lyα (Tian et al., 2009b). Figure 14 reveals clearly that most Lyβ profiles in a polar coronal hole are stronger in the blue peak, distinctly different from the well-known red-peak dominance of the Lyβ profiles in the quiet Sun (Warren et al., 1998; Xia, 2003; Curdt et al., 2008b; Tian et al., 2009d). Since the asymmetries of Lyman line profiles are believed to be at least partly determined by flows in the upper solar atmosphere (Gouttebroze et al., 1978; Fontenla et al., 2002; Gunár et al., 2008), Tian et al. (2009b) suggested that the prevailing solar wind outflow might be responsible for the blue-peak asymmetry of the Lyβ profiles in the polar coronal hole. An alternative explanation is to start with the fact that the Lyβ line behaves more or less similar to typical TR lines in the quiet Sun. In polar coronal holes, the opacity is so large that the Lyβ line now behaves more similar to Lyα and shows a stronger blue peak in its profile (Curdt & Tian, 2010).

The Lyα/Lyβ radiance ratio in coronal holes has also been investigated by Tian et al. (2009b), who found that the ratio decreases from the quiet-Sun level (~190) at disk center to about 130 at the limb. This decreasing trend could be explained by the fact that the Lyα and Lyβ lines show no and weak limb brightening, respectively.

3.4. Initial acceleration of the fast solar wind

Axford et al. (1999) suggested that the solar wind may be produced by small-scale magnetic reconnection in the network. This viewpoint has been supported by Tu et al. (2005a), who found upflowing and downflowing plasma (that is possibly related with reconnection) at a height of about 20 Mm and 5 Mm, respectively. Modeling work also supports the idea that magnetic reconnections between open funnels and cool loops aside in the chromospheric and TR network can give rise to the nascent solar wind outflow and corresponding downflows (Büchner & Nikutowski, 2005; He et al., 2008).

In the reconnection-driven model of the solar wind origin, the nascent solar wind outflow appears first in the upper TR of the coronal hole (Tu et al., 2005a; He et al., 2008). Two-dimensional images of the Doppler shift of Ne VIII obtained by the SUMER instrument revealed predominant blue shifts of the Ne VIII line, with the most prominent shifts occurring along the network lanes in polar coronal holes (Hassler et al., 1999; Wilhelm et al., 2000). These blue shifts are widely believed to be signatures of the initial outflow of the solar wind (Dammasch et al., 1999; Hassler et al., 1999; Wilhelm et al., 2000; Xia et al., 2003; Tu et al., 2005a; Aiouaz et al., 2005).

Due to the lack of strong hot lines, two-dimensional dopplergrams of emission lines with a higher formation temperature than that of Ne VIII could not be reliably derived through SUMER observations. Yet the temperature-dependent outflow, which is expected from a reconnection-driven solar wind model, was recently identified by Tian et al. (2010a) through EIS observations. Tian et al. (2010a) produced two-dimensional dopplergrams of several emission lines formed in the upper TR and lower corona of a polar coronal hole. They found that patches of significant blue shift are clearly present on the dopplergrams of emission lines with formation temperatures higher than $\log(T/\mathrm{K})$ =5.8. These patches are isolated at the upper-TR temperature, but expand in size with increasing temperature and finally merge in the corona. This result is consis-

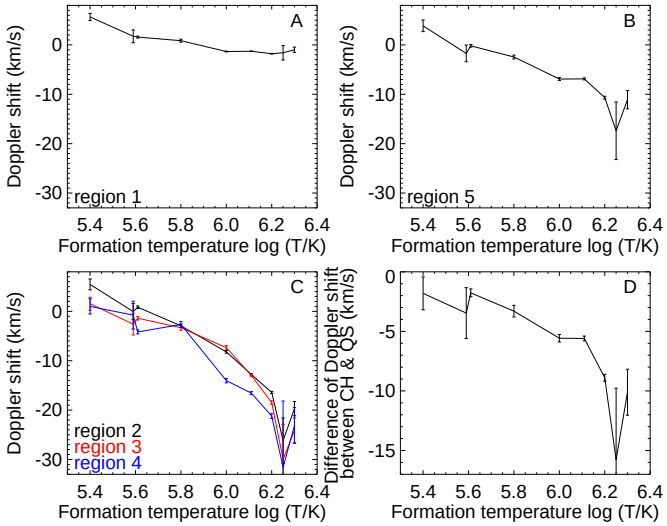

Figure 15: Temperature dependence of the Doppler shift for emission lines in a quiet-Sun region (A), a coronal-hole region (B), and three sub-regions inside the coronal hole (C). The temperature dependence of the difference between the Doppler shifts in the coronal-hole and quiet-Sun regions is shown in panel D. The error bars represent the uncertainties originating from the corresponding fitting errors of the line centers. To avoid overlapping, the data points for the Mg VI and Fe VIII lines are plotted at $\log(T/\mathrm{K}) = 5.59$ and $\log(T/\mathrm{K}) = 5.61$, respectively. Adapted from Tian et al. (2010a).

tent with the scenario of solar wind outflow being guided by expanding magnetic funnels (Tu et al., 2005a; Tian et al., 2008a).

The temperature dependence of the outflow shown in Figure 15 reveals that the Doppler shift of the quiet-Sun materials is very small and independent of the temperature, while inside the coronal hole a clear enhancement of the blue shift with increasing temperature is present in the upper TR and corona (Tian et al., 2010a). Under a simple assumption that emission lines with a higher formation temperature are formed in higher layers of the solar atmosphere, Tian et al. (2010a) concluded that the observed temperature-dependent outflow corresponds to the initial acceleration of the fast solar wind. The steady enhancement of the blue shift with temperature suggests a nearly steady acceleration process.

The temperature variation of the difference of Doppler shift between the coronal hole and quiet Sun was investigated by Xia et al. (2004) and Tian et al. (2010a). The absolute difference was found to increase with temperature from about $\log(T/\mathrm{K}) = 4.2$ to $\log(T/\mathrm{K}) = 6.3$. A significant blue shift in coronal holes with respect to the quiet Sun was clearly present even at low temperature of $\log(T/\mathrm{K}) \approx 5.2$ (Xia et al., 2004; Raju, 2009), probably indicating that an upward trend of the flows in open funnels compared to the quiet-Sun loops is already present in the middle TR.

4. Active regions

Active regions (ARs) are strong-field regions on the Sun and are the main sources of hazardous space weather events. Their emission patterns, flow fields, and plasma properties are largely different from those in the quiet Sun.

4.1. Flow field of active regions

Large-scale loop-like emission structures outlining the strong magnetic field are the dominant visible features in ARs. The loop legs are usually associated with persistent redshifts of emission lines formed in the TR and lower corona (Marsch et al., 2004; Dammasch et al., 2008; Marsch et al., 2008; Del Zanna, 2008). Steady blue shifts lasting for several days have been observed at the edges of some ARs (Marsch et al., 2004, 2008; Del Zanna, 2008; Harra et al., 2008). These flows seem to be guided by the dominant magnetic field structures and their quasi-steadyness indicates the presence of coronal convection/circulation in ARs (Marsch et al., 2008).

The redshifts associated with loop legs are considered to have an origin similar to the prominent redshifts in network lanes of the quiet Sun, although their values often reach as high as 30 km s^{-1} (Marsch et al., 2004; Dammasch et al., 2008). In the quiet Sun and coronal holes, the redshifts in network lanes are only present in middle-TR lines. While in ARs, the redshifts in loop legs are generally present in emission lines formed at middle TR to lower coronal temperatures. Observations show that the Doppler shift turns from redshift to blue shift at a temperature of $\log(T/\mathrm{K}) \approx 6.2$ (Del Zanna, 2008). The stronger magnetic field in ARs compared to the quiet Sun may result in more efficient heating of the loop legs, leading to a hotter upflowing plasma and subsequently a cooler downflowing plasma with a wider temperature range.

The blue shifts of TR and coronal lines at boundaries of some ARs, which are usually 20-50 km s^{-1} in magnitude, have been interpreted as possible signatures of the nascent slow solar wind (Marsch et al., 2008; Harra et al., 2008; He et al., 2010). These blue shifts revealed through spectroscopic observations are consistent with the outflows revealed through X-Ray imaging observations (Sakao et al., 2007). Del Zanna (2008) investigated the temperature dependence of the outflow and found a steady enhancement of the blue shift with increasing temperature. This temperature-dependent blue shift is very similar to that found by Tian et al. (2010a) in a polar coronal hole, and could be the spectroscopic signature of the initial acceleration of the slow solar wind. The temperature dependences of flare and CME-related outflows, which show dramatic changes at ~1 MK, were found by Imada et al. (2007) and Jin et al. (2009). The dramatic changes are consistent with the impulsive nature of these explosive phenomena (e.g., Chen & Shibata, 2000; Zhang et al., 2005; Chen et al., 2007; Zhang et al., 2006). Thus, the behavior of the solar wind at its origin and of the CME or flare during their initiations are distinctly different.

4.2. TR properties of sunspots and plage

Sunspots are solar features which have been studied for thousands of years (see a review by Solanki, 2003). Studies of sunspots and their surrounding plage regions are usually concentrated on their magnetic field and plasma properties in the convection zone, photosphere and chromosphere (e.g., Ichimoto et al., 2007; Katsukawa et al., 2007; Magara & Tsuneta, 2008; Watanabe et al., 2009; Li & Zhang,

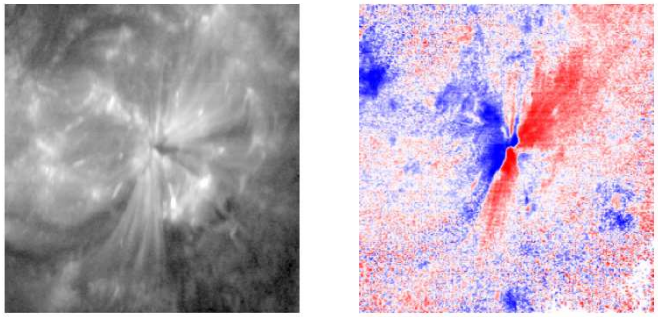

Figure 16: A sunspot and its surrounding region in Ne VIII. Left: radiance image. Right: dopplergram. Adapted from Dammasch et al. (2008).

2009). In contrast, the TR properties of sunspots and plage have been less investigated.

The most prominent structures in images of emission lines formed in the middle and upper-TR are sunspot plumes (see Figure 16) which exhibit significantly enhanced radiation at locations overlying sunspot umbrae (Foukal et al., 1974; Foukal, 1976). The strongly enhanced line emission at TR temperatures and the reduced continuum even lead to the sticking out of many normally very weak TR lines in sunspot plumes (Curdt et al., 2000; Tian et al., 2009c). A sunspot plume might be the common footpoint of several long-reaching loops, and its two end points are usually anchored respectively in the umbra and somewhere far from the sunspot (e.g., Brynildsen et al., 2001; Dammasch et al., 2008). Brosius & Landi (2005) and Tian et al. (2009c) performed a DEM analysis to compare the temperature structure between sunspot plumes and other features by using the CDS and SUMER spectra, respectively. The results are consistent with the fact that sunspot plumes have greatly enhanced emission compared to the surrounding regions in the temperature range between $\log(T/\mathrm{K})$ =5.0 and $\log(T/\mathrm{K})$ =6.0. The reason of the strong emission of sunspot plumes at these temperatures was investigated by Tian et al. (2009c), who attributed it to a large filling factor of the plume.

The average Lyman line profiles in sunspots and plage regions were presented by Tian et al. (2009c). Figure 17 shows clearly that profiles of the lower-order Lyman lines also exhibit central reversals and stronger red peaks, which are similar to those in the quiet Sun (Warren et al., 1998). However, the Lyman line profiles are almost not reversed in sunspots, especially in the sunspot plume and umbra. Although Lyα spectra have not been observed by SUMER in sunspots yet, a Lyα profile obtained by the Ultraviolet Spectrometer and Polarimeter onboard the *SMM* (Solar Maximum Mission) spacecraft seems to be flat-topped and not obviously reversed (Fontenla et al., 1988). These results imply a much smaller opacity in sunspots compared to the plage regions, and is consistent with the conclusion of Bartoe et al. (1979) and Jordan et al. (1978) that the observed strong emission of the molecular hydrogen in sunspots is caused by the excitation of the enhanced backward radiation of Lyα and O VI 1031.93 Å due to the greatly reduced opacity.

The smaller opacity in sunspots and larger opacity in plage regions are likely related to the varying Lyman emission from the chromosphere and TR. In either the plage region or quiet-Sun region, the Lyman line emission originates by a large fraction in the chromosphere and is strongly absorbed by the dense hydrogen atoms in upper layers, causing a strong central reversal of the lower order Lyman line profiles. While in sunspots, due to possibly less chromospheric material or a more extended TR, the ratio of the chromospheric to TR contributions of the Lyman line radiation is much lower. Thus, the absorption of the Lyman line emission is very weak since the density of the solar atmosphere decreases dramatically above the TR. Sunspot plumes are mainly TR features, so that the TR contribution to the Lyman line emission should dominate over the chromospheric contribution. Moreover, the loops associated with sunspot plumes are usually far reaching and large in size. The overlying corona is thus insufficiently dense to cause an obvious dip at the center of the Lyman line profiles.

The electron density of sunspot plumes has been derived by Doyle et al. (1985), Doyle & Madjarska (2003), and Brosius & Landi (2005), through observations made by the S-055 EUV spectrometer onboard *Skylab*, the SUMER and CDS instruments, respectively. The plume density was found to be about $\log(N_\mathrm{e}/\mathrm{cm}^{-3}) = 10.0$ or lower by using O V and O IV line pairs. Tian et al. (2009c) compared the electron densities of sunspots with that of the plage, and found that the densities of the umbra and plume regions are $\log(N_\mathrm{e}/\mathrm{cm}^{-3}) \approx 10$, which is not so different from the TR density of the quiet Sun (Griffiths et al., 1999) and is one order of magnitude smaller than in the plage and penumbra regions. The lower density in sunspots compared to the surrounding plage may indicate that the sunspot plasma emitting at TR temperatures is located higher up than the plasma in the surrounding plage region, since the density of the solar atmosphere decreases almost exponentially with height above the photosphere. The possibly higher TR above sunspots is consistent with the result of an independent study, showing that EUV emission lines in regions of stronger magnetic field have higher formation heights (Guo et al., 2009). This scenario also supports the temperature structure of sunspots proposed by Nicolas et al. (1982), in which the sunspot TR temperature is much lower than the surrounding temperature at the same height. Since the magnetic loops associated with sunspot plumes usually have one footpoint anchored in the umbra and the other in the plage region, the much lower density in the umbra compared to the plage could probably establish a sufficient pressure difference to initiate siphon flows along the loops and result in the persistent prominent redshifts of TR lines in sunspot plumes (Doyle & Madjarska, 2003; Tian et al., 2009c).

The different temperature structures in sunspots and the surrounding plage regions are summarized in Figure 18. The iso-temperature lines are used to mark the boundaries between two layers. A higher and more extended TR is clearly present above the sunspot than above the plage regions. In sunspot regions, the dominant flows in the photosphere and chromosphere are opposite in their directions, which are known as the Evershed flow and inverse Evershed flow (Evershed, 1909a,b). Downflows are usually observed to be associated with sunspot plumes at TR temperatures. It is still unclear

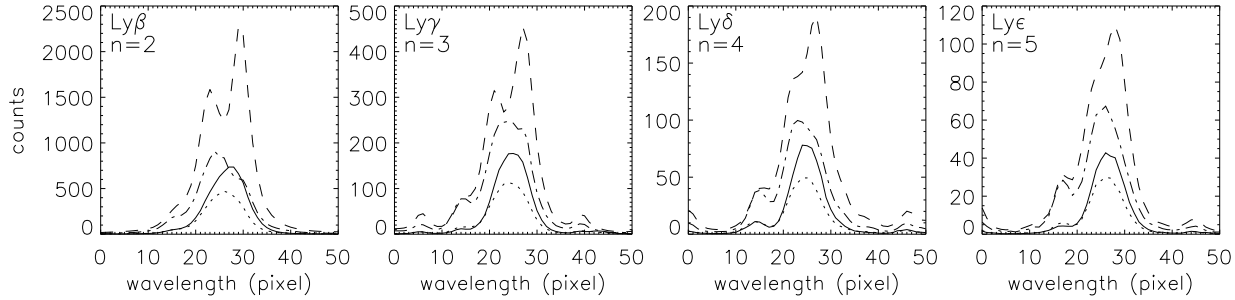

Figure 17: Typical Lyman line profiles observed in the sunspot plume (solid), umbra (dotted), penumbra (dot-dashed), and plage (dashed). Note that the profiles in the umbra have been multiplied by a factor of two. Adapted from Tian et al. (2009c).

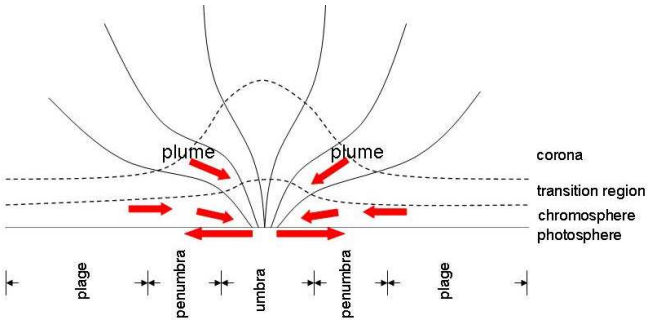

Figure 18: Schematic representation of the temperature structure in active regions. The solid lines represent magnetic field lines originating from the umbra. The dashed lines can be understood as iso-temperature lines which mark the boundaries between two adjacent layers. Arrows show the directions of flows in different layers of the solar atmosphere.

whether these downflows are the leakage of the inverse Evershed flow into the TR (Teriaca et al., 2008), or resulting from syphon flows along far-reaching loops (e.g., Brynildsen et al., 2001; Doyle & Madjarska, 2003).

5. Summary

Recent advances in the investigation of the solar TR, resulting especially from spectroscopic observations in the FUV/EUV spectral range, have been reviewed in this article. Significant progress was achieved in many aspects of the TR research, concerning the magnetic field structures and plasma properties, behaviors of the nascent solar wind and other systematic flows, and characteristics of the hydrogen Lyman line profiles in different parts of the Sun (the quiet Sun, coronal holes, and ARs).

Based on studies combining spectroscopic observations with magnetic field extrapolations, a new scenario of the TR consisting of different magnetic field and emission structures in the quiet Sun and coronal holes has been proposed. In this new picture (shown in Figure 12), the TR is higher and more extended in coronal holes than in the quiet Sun. The dominant magnetic field structures in CHs are open magnetic funnels which are related to the fast solar wind, whereas there are only low-lying magnetic loops in coronal holes. In contrast, in the quiet Sun magnetic loops with different spatial scales are crowded. Occasionally, some large loops might become locally open through magnetic reconnection, and then possibly release material to the solar wind. These different scenarios naturally lead to a strong expansion of the magnetic funnels in coronal holes and a relatively weak expansion of magnetic field structures in the quiet Sun through the upper TR.

Although the TR is believed to be a dynamic layer, quasi-steady TR flows lasting from several hours to several days have also been observed to be present in the quiet Sun, coronal holes, and ARs. In coronal holes, the predominant blue shift of emission lines was found to increase steadily from the upper TR to the lower corona, indicating the steady acceleration of the nascent fast solar wind, while in the quiet Sun the blue shifts of upper-TR lines are localized in network junctions and considered to be signatures of mass supply to large coronal loops. The persistent redshift of middle-TR lines in the network could correspond to the downflowing plasma occurring after continuous magnetic reconnections or cooling of the upflows. Persistent redshifts of emission lines formed in the TR and lower corona are usually found in the legs of AR loops, and steady blue shifts lasting for several days are often present at the boundaries of some ARs. All these flows seem to be guided by the dominant magnetic field structures, and their quasi-steadyness suggests the presence of some kind of convection/circulation in the TR and corona. Sporadically, small-scale transient flows will locally occur and be superposed on the background quasi-steady flow field.

Based on spectroscopic observations in EUV/FUV, properties of the TR above sunspots and the surrounding plage regions have also been comprehensively investigated. By comparing the Lyman line profiles, electron densities, DEM curves, and filling factors of the sunspot plume, umbra, penumbra, and the surrounding plage regions, the TR above sunspots was found to be higher and probably more extended (shown in Figure 18). The opacity of the hydrogen lines is apparently much smaller above sunspots than above plage regions. Theoretical calculations and observational inferences also indicate that the enhanced TR emission of the sunspot plume is probably caused by a large filling factor.

As the dominant emission line in the lower TR, the hydrogen Lyα line provides a good tool to diagnose through its profile the coupling between the lower-TR emission and the flows in upper-TR layers. With SUMER observations, high-

quality solar Lyα profiles without geocoronal absorption were recently obtained for the first time. As an unexpected result, this strongly self-reversed line is often asymmetric with a stronger blue peak, and there is a clear correspondence between this asymmetry and downflows in the middle TR. Profiles with deeper self-reversals were found statistically in the internetwork rather than the network. A larger peak separation indicative of a larger opacity was found in coronal holes than in the quiet Sun. The Lyβ line is also a useful line to study the coupling between the lower TR and higher layer, because of its opposite asymmetry in the quiet Sun and polar coronal holes. Signatures of TR explosive events are often clearly present in the Lyβ line.

6. Outlook

The TR is a key region to understand the mechanisms of solar wind origin and coronal heating. Although our understanding of the TR was greatly improved due to many new observations and theoretical work in the past decade, some open questions remain and need to be answered by future observations and models.

The possible solar wind origin from quiet-Sun regions is poorly understood. The opening of the magnetic loops has not been directly observed in the quiet Sun. On the other hand, although signatures of outflows are identified through TR and coronal observations and interpreted as solar wind origin in both the coronal hole and active region edges, the detailed observational evidence of the driving mechanism for the solar wind is still missing. High-cadence observations of the magnetic field structures in both the photosphere and higher layers are required to investigate the mechanisms of solar wind origin in different regions. The planned Coronal Solar Magnetism Observatory (COSMO) will provide unprecedented routine and high-cadence measurements of the magnetic fields above the photosphere, which is likely to unveil the driving mechanisms of solar wind origin in the TR and corona.

Although we know that the TR is the interface between the cool chromosphere and hot corona, the detailed link between the chromosphere and corona is in fact not well understood. This is partly because of the moderate spatial and temporal resolutions of EUV/FUV observations made by current instruments. Recent observations seem to suggest that the intermittent dynamics in the upper chromosphere could drive mass ejections at TR and coronal temperatures, and thus could perhaps provide information on the missing link between the cool chromosphere and hot corona (De Pontieu et al., 2009; McIntosh & De Pontieu, 2009a,b). Such jets and spicules are small-scale transient phenomena, and current EUV/FUV observations are difficult to fully resolve them. The IRIS (Interface Region Imaging Spectrograph) mission which will be launched at the end of 2012 can provide UV spectra and images with very high spatial resolution (0.33″) in very high time cadence ($\sim$1 s), and thus will undoubtedly make a great contribution to the studies of the dynamics in the chromosphere and TR.

Our new observations of the relationship between the Lyman line asymmetries and TR flows or dynamics also need to be physically understood. Moreover, the newly observed genuine Lyα radiance profiles provide new constraints to models of the solar atmosphere. Thus, new atmospheric models including calculations of non-LTE (local thermodynamic equilibrium) radiative transfer should be developed and compared with the new observations. In addition, our understanding of the Lyα line characteristics and its role in the energy transport of the solar atmosphere will be further improved through observations by future missions such as Solar Orbiter.

Finally, since the Sun is the only star that we can spatially resolve, detailed observations of the solar TR and corona could help us understand observational results of solar-like stars and other astrophysical systems. It has been demonstrated that the structure of accretion disks around stellar-mass black holes is similar to that of the solar atmosphere (Zhang et al., 2000). Many phenomena such as collimated outflows and flares which are often observed in the solar TR and corona also occur in other astrophysical systems (see a review by Zhang, 2007). The potential value of the observed high quality full-Sun FUV/EUV spectra for the stellar studies has also been discussed by Peter (2006). In the future, we hope that our new views on the emission and structure of the solar TR could also be used for reference when investigating stellar coronae and other ultraviolet emitting astrophysical plasmas.

Acknowledgments

SUMER and MDI are instruments onboard SOHO, an ESA and NASA mission. The SUMER project is financially supported by DLR, CNES, NASA, and the ESA PRODEX programme (Swiss contribution). EIS is an instrument onboard *Hinode*, a Japanese mission developed and launched by ISAS/JAXA, with NAOJ as domestic partner and NASA and STFC (UK) as international partners. It is operated by these agencies in cooperation with ESA and NSC (Norway).

We appreciate the fruitful collaborations with Dr. L. Teriaca, Dr. E. Landi, Dr. U. Schühle, Prof. L.-D. Xia, Dr. P. Lemaire, Prof. B. N. Dwivedi, Prof. J.-C. Vial, and Dr. M. Zhang. Hui Tian thanks the long-lasting support from the Graduate School of Peking University (especially from Mr. Feng He) and from the IMPRS Research School (especially from Dr. Dieter Schmitt and Prof. Sami Solanki) run jointly by the Max Planck Society and the Universities of Göttingen and Braunschweig. The support by China Scholarship Council for Hui Tian's stay at Max-Planck-Institut für Sonnensystemforschung from September 2007 to September 2008 is also acknowledged.

Prof. Chuanyi Tu's group at Peking University are supported by the National Natural Science Foundation of China under contracts 40874090, 40931055, and 40890162. They are also supported by the Beijing Education Project XK100010404, the Fundamental Research Funds for the Central Universities, and the National Basic Research Program of China under grant G2006CB806305.

Aiouaz, T., Peter, H., & Lemaire P. 2008, A&A, 435, 713
Aiouaz, T. 2008, ApJ, 674, 1144
Athay, R. G. 1982, ApJ, 263, 982
Athay, R. G. 1984, ApJ, 287, 412

Axford, W. I., Mckenzie, J. F., & Sukhorukova, G. V. 1999, Space Science Reviews, 87, 25
Bartoe, J.-D. F., & Brueckner, G. E., 1975, Journal of the Optical Society of America, 65, 13
Bartoe, J.-D. F., Brueckner, G. E., Purcell, J. D., & Tousey, R. 1977, Appl. Opt., 16, 879
Bartoe, J.-D. F., Brueckner, G. E., Nicolas, K. R., et al. 1979, MNRAS, 187, 463
Basri, G. S., Linsky, J. L., Bartoe, J.-D. F., et al. 1979, ApJ 230, 924
Bocchialini, K., & Vial, J.-C. 1996, Sol. Phys. 168, 37
Bohlin, J. D., Vogel, S. N., Purcell, J. D., et al. 1975, ApJ, 197, L133
Bonnet, R. M. 1981, Space. Sci. Rev., 29, 131
Brekke, P., Hassler, D. M., & Wilhelm, K. 1997, Sol. Phys., 175, 349
Brosius, J. W., & Landi, E. 2005, ApJ, 632, 1196
Brosius, J. W., Rabin, D. M., & Thomas, R. J. 2007, ApJ, 656, L41
Brosius, J. W., Rabin, D. M., Thomas, R. J., & Landi, E. 2008, ApJ, 677, 781
Brown, D. S., Parnell, C. E., DeLuca, E. E., Golub L., & Mcmullen, R. A. 2001, Sol. Phys., 201, 305
Brueckner, G. E., & Bartoe, J.-D. F., 1974, Sol. Phys., 38, 133
Brueckner,G. E., & Bartoe, J.-D. F., 1983, ApJ, 272, 329
Brueckner, G. E., Bartoe, J.-D. F., Cook, J. W., Dere, K. P., & Socker, D. G. 1986, Adv. Space Res., 6, 263
Brynildsen, N., Maltby, P., Fredvik, T., et al. 2001, Sol. Phys., 198, 89
Büchner, J., & Nikutowski, B. 2005, ESA SP-592, 141
Büchner, J. 2006, Space Science Reviews, 122, 149
Chae, J., Wang, H., Lee, C. Y., et al. 1998a, ApJ, 497, L109
Chae, J., Schühle, U., Lemaire, P. 1998b, ApJ, 505, 957
Chae, J., Yun, H. S., & Poland, A. I. 1998c, ApJS, 114, 151
Chen, P. F., & Shibata, K. 2000, ApJ, 545, 524
Chen, P. F., & Priest, E. R. 2006, Sol. Phys., 238, 313
Chen, Y., Hu, Y. Q., & Sun, S. J. 2007, ApJ, 665, 1421
Culhane, J. L., et al. 2007, Sol. Phys., 243, 19
Curdt, W., Dwivedi, B. N, & Feldman, U. 2000, J. Astrophys. Astr. 21, 397
Curdt, W., Brekke, P., Feldman, U., Wilhelm, K., Dwivedi, B. N., Schühle, U., & Lemaire, P. 2001, A&A 375, 591.
Curdt, W., Landi, E., & Feldman, U. 2004, A&A, 427,1045
Curdt, W., Tian, H., Dwivedi, B. N., & Marsch, E. 2008a, A&A, 491, L13
Curdt, W., Tian, H., Teriaca, L., Schühle, U., & Lemaire, P. 2008b, A&A, 492, L9
Curdt, W., Tian, H., Teriaca, L., & Schühle, U. 2010, A&A, 511, L4
Curdt, W., & Tian, H., Proceedings of SOHO-23, 2010, in press
Dammasch, I. E., Wilhelm, K., Curdt, W., & Hassler, D. M. 1999, A&A, 346, 285
Dammasch, I. E., Curdt, W., Dwivedi, B. N., & Parenti, S. 2008, Annales Geophysicae, 26, 2955
Del Zanna, G. 2008, A&A, 481, L49
De Pontieu, B., McIntosh, S. W., Hansteen, V. H., et al. 2009, ApJ, 701, L1
Dere, K. P., Bartoe, J.-D. F., Brueckner, G. E. 1989, Sol. Phys., 123, 41
Dere, K. P. 2008, A&A, 491, 561
Dere, K. P. 2009, A&A, 497, 287
Doschek, G. A., Bohlin, J. D., & Feldman, U. 1976, ApJ, 205, L177
Doschek, G. A., Mariska, J. T., & Akiyama, S. 2004, ApJ, 609, 1153
Doschek, G. A., Landi, E., Warren, H. P., & Harra, L. K. 2010, ApJ, 710, 1806
Dowdy, J. F., Jr., Rabin, D., & Moore, R. L. 1986, Sol. Phys., 105, 35
Doyle, J. G., Raymond, J. C., Noyes, R. W., & Kingston, A. E. 1985, ApJ, 297, 816
Doyle, J. G., & Madjarska, M. S. 2003, A&A, 407, L29
Doyle, J. G., Roussev, I. I., & Madjarska, M. S. 2004, A&A, 418, L9
Doyle, J. G., Popescu, M. D., & Taroyan, Y. 2006, A&A., 446, 327
Evershed, J. 1909a, MNRAS, 69, 454
Evershed, J. 1909b, The Observatory, 32, 291
Falconer, D. A., Moore, R. L., Porter, J. G., & Hathaway, D. H. 1998, ApJ, 501, 386
Fang, C., Feautrier, N., & Hénoux, J.-C. 1995, A&A, 297, 854
Feldman, U. 1983, ApJ, 275, 367
Feldman, U. 1987, ApJ, 320, 426
Feldman, U., & Laming, J. M. 1994, ApJ, 434, 370
Fontenla, J. M., Reichmann, E. J., & Tandberg-Hanssen, E. 1988, ApJ 329, 464
Fontenla, J. M., Avrett, E. H., & Loeser, E. 2002, ApJ 572, 636
Foukal, P. V., Huber, M. C. E., Noyes, R. W., et al. 1974, ApJ, 193, L143
Foukal, P. V. 1976, ApJ, 210, 575
Foukal, P., 1978, ApJ, 223, 1046
Gabriel, A. H. 1976, Philos. Trans. R. Soc. London A, 28l, 575
Golub, L., Krieger, A. S., Silk, J. K., Timothy, A. F., & Vaiana, G. S. 1974, ApJ, 189, L93
Gontikakis, C., Peter, H., Dara, H. C. 2003, A&A,408,743
Gouttebroze, P., Lemaire, P., Vial, J.-C., & Artzner, G. 1978, ApJ, 225, 655
Gouttebroze, P., Heinzel, P., & Vial, J. C. 1993, A&AS, 99, 513
Griffiths, N. W., Fisher, G. H., Woods, D. T., & Siegmund, O. H. W. 1999, ApJ, 512,992
Gunár, S., Heinzel, P., Anzer,U., & Schmieder, B., 2008, A&A, 490, 307
Guo, Y., Ding, M. D., Jin, M., & Wiegelmann, T. 2009, ApJ, 696, 1526
Habbal. S. R., Dowdy, J. F. Jr., & Withbroe, G. L. 1990, ApJ, 352, 333
Hansteen, V. 1993, ApJ, 402, 741
Hansteen, V., Maltby, P., & Malagoli, A. 1997, Astronomical Society of the Pacific Conference Series, 111, 116
Harra, L. K., et al. 2008, ApJ, 676, L147
Harrison, R. A., et al. 1995, Sol. Phys., 162, 233
Harrison, R. A. 1997, Sol. Phys., 175, 467
Hassler, D. M., Dammasch, I. E., Lemaire, P., Brekke, P., Curdt, W., Mason, H. E., Vial, J.-C., & Wilhelm, K. 1999, Science, 283, 810
He, J.-S., Tu, C.-Y., & Marsch, E. 2007, A&A, 468, 307
He, J.-S., Tu, C.-Y., & Marsch, E. 2008, Sol. Phys., 250, 147
He, J.-S., Tu, C.-Y., Tian, H., & Marsch, E. 2009, Advances in space research, 45, 303
He, J.-S., Marsch, E., Tu, C.-Y., Guo, L.-J., & Tian, H. 2010, A&A, in press
Heinzel, P., Anzer, U., & Gunár, S. 2005, A&A, 442, 331
Hénoux, J.-C., Fang, C., & Gan, W.-Q., 1995, A&A, 297, 574.
Ichimoto, K., et al. 2007, Science, 318, 1597
Imada, S., et al. 2007, PASJ, 59, S793
Innes, D. E., Brekke, P., Germerott, D., et al. 1997a, Sol. Phys., 175, 341
Innes, D. E., Inhester, B., Axford, W. I., et al. 1997b, Nature, 386
Jin, M., Ding, M. D., Chen, P. F., Fang, C., & Imada, S. 2009, ApJ, 702, 27
Jordan, C., Brueckner, G. E., Bartoe, J.-D. F., et al. 1978, ApJ, 226, 687
Katsukawa, Y., et al. 2007, Science, 318, 1594
Kneer, F., et al. 1981, Sol. Phys., 69, 289
Lemaire, P., Charra, J., Jouchoux, A., et al. 1978, ApJ, 223, L55
Lemaire P., et al. 1997, Sol. Phys., 170, 105
Lemaire, P., Emerich, C., Vial, J.-C., Curdt, W., Schühle, U., & Wilhelm, K. 2005, Adv. Space Res., 35, 384
Li, L.-P., & Zhang, J. 2009, ApJ, 706, L17
Liu, Y., & Lin, H. 2008, ApJ, 680, 1496
Longcope, D. W. 1998, ApJ, 507, 433
Madjarska, M. S., & Doyle, J. G. 2002, A&A, 382, 319
Madjarska, M. S., Doyle, J. G., Teriaca, L., & Banerjee, D. 2003, A&A, 398, 775
Magara, T, & Tsuneta, S. 2008, PASJ, 60, 1181
Mariska, J. T. 1988, ApJ, 334, 489
Mariska, J. T. 1992, The solar transition region, Cambridge University Press
Marsch, E., Tu, C.-Y., Heinzel, P., Wilhelm, K., & Curdt, W. 1999, A&A, 347, 676
Marsch, E., Tu,C.-Y., & Wilhelm, K. 2000, A&A, 359, 381
Marsch, E., Antonucci, E., Bochsler, P., et al. 2002, Advances in Space Research, 29, 2027
Marsch, E., Wiegelmann, T., & Xia, L. D. 2004, A&A, 428, 629
Marsch, E., Zhou, G.-Q., He, J.-S., & Tu, C.-Y. 2006, A&A, 457, 699
Marsch, E., Tian, H., Sun, J., Curdt, W., & Wiegelmann, T. 2008, ApJ, 684, 1262
McAteer, R. T. J. 2004, Ph.D. Thesis (Belfast: Queen's University of Belfast)
McClymont, A. N., & Craig, I. J. D. 1987, ApJ, 312, 402
McIntosh, S. W. 2007a, ApJ, 670, 1401
McIntosh, S. W., et al. 2007b, ApJ, 654, 650
McIntosh, S. W., & De Pontieu, B. 2009a, ApJ, 706, L80
McIntosh, S. W., & De Pontieu, B. 2009b, ApJ, 707, 524
Metcalf, T. R., Jiao, L., McClymont, A. N., & Canfield, R. C. 1995, ApJ, 439, 474
Nicolas, K. R., Kjeldseth Moe, O., & Tousey, R. 1976, JGR, 81(19), 3465
Nicolas, K. R., Kjeldseth-Moe, O., Bartoe, J.-D. F., & Brueckner, G. E. 1982, Sol. Phys., 81, 253
Parnell, C. E., Priest, Eric R., & Titov, V. S. 1994, Sol. Phys., 153, 217
Patsourakos, S., Vial, J.-C., Gabriel, A. H., & Bellamine, N. 1999, ApJ, 522, 540

Peter, H., & Judge, P. G. 1999, ApJ, 522, 1148
Peter, H. 2001, A&A, 374, 1108
Peter, H., & Vocks, C. 2003, A&A, 411, L481
Peter, H. 2004, Reviews in Modern Astronomy, 17, 87
Peter, H. 2006, A&A, 449, 759
Popescu, M. D., Doyle, J. G., & Xia, L. D. 2004, A&A, 421,339
Priest, E. R., Parnell, C. E., & Martin, S. F. 1994, ApJ, 427, 459
Raju, K. P. 2009, Sol. Phys., 255, 119
Ravindra, B., & Venkatakrishnan, P. 2003, Sol. Phys., 215, 239
Reeves, E. M. 1976, Sol. Phys., 46, 53
Santos, J. C., & Büchner, J. 2007, Astrophys. Space Sci. Trans., 3, 29
Sakao, T., et al. 2007, Science, 318, 1585
Schrijver, C. J., Sandman, A. W., Aschwanden, M. J., & deRosa, M. L. 2004, ApJ, 615, 512
Schmieder, B., Gunár, S., Heinzel, P., Anzer, U. 2007, Sol. Phys. 241, 53
Seehafer, N. 1978, Sol. Phys., 58, 215
Sheeley, N. R. Jr., & Golub, L. 1979, Sol. Phys., 63, 119
Solanki, S. K. 2003, Astron. Astrophys. Rev., 11, 153
Stucki, K., Solanki, S. K., & Schühle, U., et al. 2000, A&A, 363, 1145
Teriaca, L., Banerjee, D., & Doyle, J. G. 1999, A&A, 349, 636
Teriaca, L., Banerjee, D., Falchi, A., et al. 2004, A&A, 427, 1065
Teriaca, L., Schühle, U., Solanki, S. K., et al. 2005a, ESA SP-596, 66
Teriaca, L., Schühle, U., Solanki, S. K., et al. 2005b, ESA SP-600, 100
Teriaca, L., Schühle, U., Solanki, S. K., et al. 2006, ESA SP-617, 77
Teriaca, L., Curdt, W., & Solanki, S. K. 2008, A&A, 491, L5
Tian, H., Tu, C.-Y., He, J.-S., & Marsch, E. 2007, Adv. Space Res., 39, 1853
Tian, H., Tu, C.-Y., Marsch, E., He, J.-S., Zhou, G.-Q. 2008a, A&A, 478, 915
Tian, H., Marsch, E., Tu, C.-Y., Xia, L.-D.,& He, J.-S. 2008b, A&A, 482, 267
Tian, H., Xia, L.-D., He, J.-S., Tan, B., & Yao, S. 2008c, Chin. J. Astron. Astrophys., 8, 732
Tian, H., Curdt, W., Marsch, E., & He, J.-S. 2008d, ApJ, 681, L121
Tian, H., Tu, C.-Y., Xia, L.-D.,& He, J.-S. 2008e, A&A, 489, 1297
Tian, H., Marsch, E., Curdt, W., & He, J.-S. 2009a, ApJ, 704, 883
Tian, H., Teriaca, L., Curdt, W., & Vial, J.-C. 2009b, ApJ, 703, L152
Tian, H., Curdt, W., Teriaca, L., Landi, E., & Marsch, E. 2009c, A&A, 505, 307
Tian, H., Curdt, W., Marsch, E., & Schühle, U. 2009d, A&A, 504, 239
Tian, H., Tu, C.-Y., Marsch, E., He, J.-S., & Kamio, S. 2010a, ApJ, 709, L88
Tian, H., Tu, C.-Y., Marsch, E., He, J.-S., Zhou, C., & Zhao, L. 2010b, Solar Wind 12 Proceedings, AIP, 1216, 36
Tu, C.-Y., Zhou, C., Marsch, E., Xia, L.-D., Zhao, L., Wang, J.-X., & Wilhelm, K. 2005a, Science, 308, 519
Tu, C.-Y., Zhou, C., Marsch, E., Wilhelm, K., Zhao, L., Xia, L.-D., & Wang, J.-X. 2005b, ApJ, 624, L133
Tu, C.-Y., Schwenn, R., Donovan, E., et al. 2008, Advances in Space Research, 41, 190
Ugarte-Urra, I., Doyle, J. G., Madjarska, M. S., & O′Shea, E. 2004a, A&A, 418, 313
Ugarte-Urra, I., Doyle, J. G., Madjarska, M. S., & Foley, C. R. 2004b, A&A, 425, 1083
Ugarte-Urra, I., Doyle, J. G., & Del Zanna G. 2005, A&A, 435, 1169
Vernazza, J. E., & Reeves, E. M. 1978, ApJS, 37, 485
Vernazza, J. E., Avrett, E. H., & Loeser, R. 1981, ApJS, 45, 635
Vial, J.-C. 1982, ApJ, 253, 330
Vial, J.-C., Ebadi, H., & Ajabshirizadeh, A. 2007, Sol. Phys. 246, 327
Vial, J.-C., Auchère, F., Chang, J., Fang, C., et al. 2008, Advances in Space Research, 41, 183
Wang, Y.-M., Sheeley, N. R., Jr., & Nash, A. G. 1990, Nature, 347, 439
Wang, Y.-M. 2009, Space Sci. Rev., 144, 383
Warren, H. P., Mariska, J. T., & Wilhelm, K. 1998, ApJS 119, 105
Watanabe, H., Kitai, R., & Ichimoto, K. 2009, ApJ, 702, 1048
Webb, D. F., Martin, S. F., Moses, D., & Harvey, J. W. 1993, Sol. Phys., 144, 15
Wiegelmann, T., Neukirch, T. 2002, Sol. Phys., 208, 233
Wiegelmann, T. and Solanki, S. K. 2004, Sol. Phys., 225, 227
Wiegelmann, T., Xia, L. D., & Marsch, E. 2005, A&A, 432, L1
Wilhelm, K., et al., 1995, Sol. Phys. 162, 189
Wilhelm, K., Lemaire, P., Dammasch, I. E., et al. 1998, A&A, 334, 685
Wilhelm, K., Dammasch, I. E., Marsch, E., & Hassler D. M. 2000, A&A, 353, 749
Wilhelm, K., Dwivedi, B.N., Marsch, E., & Feldman, U. 2004, Space. Sci. Rev., 111, 415
Wilhelm, K., Marsch, E., Dwivedi, B. N., & Feldman, U. 2007, Space. Sci. Rev., 133, 103
Xia, L.-D. 2003, Ph.D. Thesis (Göttingen: Georg-August-Univ.)
Xia, L.-D., Marsch, E., & Curdt, W. 2003, A&A, 399, L5
Xia, L.-D., Marsch, E., & Wilhelm, K. 2004, A&A, 424, 1025
Xia, L.-D., Popescu, M. D., Doyle, J. G., & Giannikakis, J. 2005, A&A, 438, 1115
Xu, Z., Fang, C., & Gan, W. 2005, Chin. J. Astron. Astrophys., 5, 519
Zhang, J., Kundu, M. R., & White, S. M. 2001, Sol. Phys., 198, 347
Zhang, J., Ma, J., & Wang, H. 2006, ApJ, 649, 464
Zhang, M., & Low, B. C. 2005, Annu. Rev. Astron. Astrophys., 43, 103
Zhang, M., Xia, L.-D., Tian, H., & Chen, Y. 2010, A&A, submitted
Zhang, S.-N., et al. 2000, Science, 287, 1239
Zhang, S.-N. 2007, Highlights of Astronomy, 14, 41
Zhang, Y. Z., Wang, J. X., & Hu, Y. Q. 2006, ApJ, 641, 572